Pergamon

Chaos, Solitons & Fractals Vol. 7, No. 2, pp. 217–246, 1996

0960-0779/96 $15.00 + 0.00

0960-0779(95)00046-1

Symbolic Dynamics of the Lorenz Equations

HAI-PING FANG*

Institute of Theoretical Physics, Academia Sinica, P.O. Box 2735, Beijing 100080, China

and

BAI-LIN HAO†

International Centre for Theoretical Physics, P.O. Box 586, 34100 Trieste, Italy

(Accepted 5 May 1995)

Abstract—The Lorenz equations are investigated in a wide range of parameters by using the method of symbolic dynamics. First, the systematics of stable periodic orbits in the Lorenz equations is compared with that of the one-dimensional (1D) cubic map, which shares the same discrete symmetry with the Lorenz model. It encompasses all the known periodic windows of the Lorenz equations with only one exception. Second, in order to justify the above approach and to understand the exceptions, another 1D map with a discontinuity is extracted from an extension of the geometric Lorenz attractor and its symbolic dynamics is constructed. All this has to be done in the light of symbolic dynamics of two-dimensional maps. Finally, symbolic dynamics for the actual Poincaré return map of the Lorenz equations is constructed in a heuristic way. New periodic windows of the Lorenz equations and their parameters can be predicted from this symbolic dynamics in combination with the 1D cubic map. The extended geometric 2D Lorenz map and the 1D antisymmetric map with a discontinuity describe the topological aspects of the Lorenz equations to high accuracy.

1. INTRODUCTON

The Lorenz equations

$$\begin{aligned} \dot{x} &= \sigma(y - x), \\ \dot{y} &= rx - xz - y, \\ \dot{z} &= xy - bz, \end{aligned} \tag{1}$$

where σ, r, b are positive parameters, corresponding to the Prandtl number, the Rayleigh number, and a geometric ratio, respectively, were first derived from a model of thermal convection between two infinite plates by B. Saltzman and E. N. Lorenz in the early 1960s [1, 2]. A few other physical problems are also known to yield the same set of equations, see, e.g. the monograph by C. Sparrow [3]. Being one of the first examples exhibiting a strange attractor in dynamical systems, this system has become a touchstone for many new ideas in chaotic dynamics. A number of interesting phenomena such as preturbulence, long transient chaos, noisy-periodicity and intermittency, has been first observed and interpreted in these equations.

*Permanent address: Department of Physics, Fudan University, Shanghai 200433, China.
†Permanent address: The Institute of Theoretical Physics, P.O. Box 2735, Beijing 100080, China.

The equations (1) are invariant under the transform

$$\begin{aligned} x &\to -x, \\ y &\to -y, \\ z &\to z. \end{aligned} \tag{2}$$

This symmetry hints on a closer relation of the Lorenz equations to the one-dimensional antisymmetric cubic map

$$x_{n+1} = h(A, x_n) \equiv Ax_n^3 + (1 - A)x_n, \tag{3}$$

where $x \in [-1, 1]$ and the parameter $A \in [1, 4]$. Indeed, a comparison of the systematics of stable periodic orbits in the Lorenz system with that of the map (3), using symbolic dynamics of three letters, has led to somewhat surprising results: 47 out of 53 primitive stable periods were described and ordered just as periodic orbits in the cubic map (3) [4]. (By primitive periodic orbits we understand those that do not come from period-doubling.) The present paper corrects the 6 non-cubic words and extends the figure to 67 with only one exception.

We mention in passing that a by-product of the study consists in that now we know the absolute nomenclature of stable periods in the Lorenz equations. Being an autonomous system, there does not exist a fixed reference time, in whose units one can measure other periods. Therefore, in all 150 and odd papers on the Lorenz equations no authors have used, e.g. 'period 5' to name an observed orbit. However, the symbolic dynamics description automatically furnishes these periods, which in turn coincide with that obtained in an extensive power spectra study of the Lorenz equations [5].

In a sense, these results are too good to be expected. One may ask many questions. Why does symbolic dynamics of a one-dimensional map work so well for a system of differential equations? Why did many words, allowed in the cubic map, not appear in the Lorenz equations? Where should one look for non-cubic words in the Lorenz equations and how to understand these exceptional cases? Can one predict new periodic orbits which should exist in a certain parameter range? Essentially, these problems may be elucidated only by invoking symbolic dynamics of two-dimensional mappings, as Poincaré maps for the Lorenz equations are actually two-dimensional.

In the meantime our understanding of symbolic dynamics of one-dimensional maps with multiple critical points and discontinuities has deepened significantly, see, e.g. [6, 7]. Symbolic dynamics of two-dimensional maps, such as the Hénon map [8–13], the Lozi map [14–16], and the Tél map [17, 18], has also been developed. Equipped with all this knowledge, we are now in a better position to answer the aforementioned questions on the Lorenz equations.

So far, most of the numerical and analytical studies on the Lorenz equations have been restricted to a one-parameter sub-family, defined by the straight line $\sigma = 10$, $b = 8/3$, and $r > 0$ in the parameter space. Another sub-family, along the line $\sigma = 16$, $b = 4$, and $r > 0$, was investigated mainly by Japanese authors [19], but did not lead to a qualitatively new picture. Early knowledge on the Lorenz equations has been extensively reviewed in a monograph [3]. We summarize some of the known results along the first parameter line for further reference.

The origin $(x, y, z) = (0, 0, 0)$ is globally attracting for $r < 1$. At $r = 1$ the origin loses stability and a pair of fixed points

$$q^{\pm} = (\pm\sqrt{(b(r - 1))} \pm \sqrt{(b(r - 1))}, (r - 1)), \tag{4}$$

appears. For $1 < r < r_0 = 13.926$ every trajectory approaches one of the fixed points. At

$r_0 = 13.926$ the first homoclinic explosion takes place and there appears an invariant set which includes a countably infinite number of periodic orbits, an uncountable number of aperiodic orbits, and an uncountable number of initial values, which are eventually attracted to the origin. For $r > r_0$ the above invariant set remains qualitatively unchanged.

For $r = r_A = 24.06$ another transition takes place. The invariant set becomes a strange attractor. In addition, an infinite sequence of homoclinic explosions begins at this r value. For $r_A < r < r_H = 24.74$ there exist a stable chaotic attractor and a pair of stable fixed points. At $r_H = 24.74$, both $q^{\pm}$ become unstable. For $r > r_H$ no stable fixed points exist any more. For $r > r_1 = 30.1$ stable periodic orbits may appear. We will concentrate on the dynamics for a wide range of $r > r_H = 24.74$.

Perhaps, J. Guckenheimer and R. Williams [20–22] were the first to apply symbolic dynamics to the Lorenz equations. For the parameter value $\sigma = 10$, $b = 8/3$, and $r \approx 28$, they gave a geometric description of a flow, based upon an examination of the Poincaré return map F of the 'rectangle' Σ, contained in the plane $z = r - 1$, as shown in Figure 5.7.1 of [22]. The rectangle Σ has opposite sides which pass through the equilibrium points q^- and q^+. In addition, $\dot{z} < 0$ at all interior points of Σ, so Σ is a cross-section for the flow. The Σ plane has been used by many authors since all the interesting trajectories intersect this plane. Guckenheimer and Williams suggested a 'geometric Lorenz attractor' G_g which should grasp the essential, topological feature of the Lorenz equations. A one-dimensional map $f_g(u_g)$, shown schematically in Fig. 15, is then extracted from the geometric attractor. We attach a subscript g to distinguish it from another one-dimensional map $f(u)$, shown in Fig. 9, which will be deduced from an 'extended geometric Lorenz attractor' G to be suggested in this paper. Guckenheimer and Williams studied the structure of orbits in the phase space by using a one-dimensional symbolic representation of the map $f_g(u_g)$.

Y. Aizawa [23] used symbolic dynamics to Lorenz equations in the context of intermittency. His approach was related to an extension of the maximal z map of Lorenz [2] to higher values of the parameter r and was less relevant to our work.

In his monograph [3] C. Sparrow introduced a two-symbol system using x and y: an orbit is assigned a letter x every time it makes a revolution around the fixed point q^+, while a letter y indicates a revolution around the fixed point q^-. Consecutive revolutions around one and the same fixed point is indicated by a power, e.g. $x^2y = xxy$. In Section 3 we will indicate the relation between this symbolic description with our symbolic dynamics.

This paper is based on a great amount of numerical data and on our knowledge of symbolic dynamics of one- and two-dimensional maps. In order to avoid any confusion of terms we list below the maps to be dealt with in this paper.

1. The simple continuous 1D antisymmetric cubic map (3).
2. A two-dimensional antisymmetric cubic map (10) or its piecewise linear counterpart (13), used to introduce concepts and notations of two-dimensional symbolic dynamics.
3. The geometric Lorenz attractor G_g, extracted from the Lorenz map F at $r \approx 28$ by making some geometric assumptions [see, e.g. [22] and the 1D Lorenz-type map $f_g(u_g)$, inferred from the former.
4. An extended geometric Lorenz map G and its associated 1D map $f(u)$, inferred from the Lorenz map F at higher values of r, say, $r > 46$, in much the same way by making further geometric assumptions.
5. The actual return map F in the Poincaré section Σ, taken at $z = r - 1$. In the following we will refer to F as the Lorenz map. Our final goal is to suggest a workable symbolic dynamics for the Lorenz map F.

We will take a physicist's approach to the problem and rely more on numerical evidence, rather than attempt to do mathematics ourselves.

The paper is organized as follows. Section 2 summarizes briefly symbolic dynamics of the one-dimensional antisymmetric cubic map (3). Then a detailed comparison between the systematics of the periodic windows in the Lorenz equations and that of map (3) is presented in Section 3. Being the main body of this paper, Section 5 consists of four parts. In Section 5.1, the two-dimensional 'extended geometric Lorenz map' G is extracted from an examination of the Lorenz map F in different parameter ranges. The symbolic dynamics of this map is identical to that of the one-dimensional map $f(u)$, shown in Fig. 9. In Section 5.2 an explicit two-dimensional representation of the symbolic dynamics for the Lorenz map F is constructed. Based on this map, we can predict whether a trajectory exists or not in the Lorenz equations. This is verified for stable periodic orbits up to length six in Section 5.3. Section 5.4 discusses the relation between the extended geometric Lorenz attractor with the geometric Lorenz attractor of Guckenheimer and Williams. We conclude with a discussion in Section 6.

2. THE ANTISYMMETRIC CUBIC MAP

The cubic map (3) maps the interval $[-1, 1]$ into itself when A varies in $[1, 4]$. The shape of $h(A, x)$ is shown in Fig. 1 where $\bar{C}$, C denote the two critical points, which divide the interval $[-1, 1]$ into three subintervals, labeled by L, M, and R, respectively, thus leading to a ternary partition by the map. The function $h(A, x)$ behaves monotonically on these subintervals. We assign a positive (+ or even) parity to the monotone increasing branches h_R and h_L as well as to the corresponding branches of the inverse function $R(y) \equiv h_R^{-1}(y)$ and $L(y) \equiv h_L^{-1}(y)$. Here we have used the same letter to denote the subinterval and the inverse function on it, a useful convention in practice. Similarly, a negative (− or odd) parity is assigned to h_M and $M(y) \equiv h_M^{-1}(y)$.

Owing to the antisymmetric property, there are two kinds of periodic orbits, symmetric

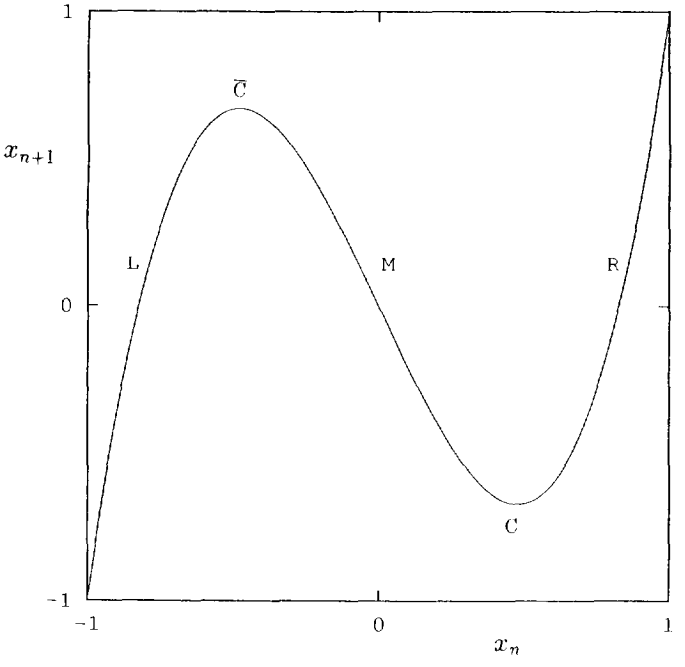

Fig. 1. The shape of the one-dimensional antisymmetric map.

and asymmetric ones. A symmetric periodic orbit satisfies $h^{(n/2)}(A, x) = -x$, n being the length of the orbit and x being a point in the orbit; asymmetric orbits do not satisfy the above relation.

Symbolically, each point x in an orbit can be labeled by one of the five letters L, $\bar{C}$, M, C, or R, according to whether it satisfies $x < \bar{C}$, $x = \bar{C}$, $\bar{C} < x < C$, $x = C$, or $x > C$. A symmetric superstable orbit, which starts from $\bar{C}$, corresponds to a symbolic sequence

$$\bar{C}\sigma_1\sigma_2 \cdots \sigma_n C\overline{\sigma_1\sigma_2} \cdots \overline{\sigma_n}\bar{C} \equiv \bar{C}PC\overline{PC},$$

where σ_i is either L or M or R; $\overline{\sigma_i}$ is the conjugate of σ_i, obtained by interchanging L and R, but leaving M unchanged. Similarly, an asymmetric superstable cycle looks like

$$\bar{C}\sigma_1\sigma_2 \cdots \sigma_n\bar{C} \equiv \bar{C}P\bar{C}.$$

We omit $\bar{C}$ hereafter as understood and simply call P a pattern or a word.

Given two patterns $P_1 = P^*\sigma$ and $P_2 = P^*\mu$, where P^* denotes their common leading string and $\sigma \neq \mu$, an order is defined in the following way.

First, there is a natural order

$$L < \bar{C} < M < C < R \tag{5}$$

on the interval I. Being different letters, σ and μ must have been ordered according to (5).

Second, if P^* contains an even number of M (we simply say P^* is even), then $P_2 > P_1$ if $\mu > \sigma$, and $P_2 < P_1$ otherwise. If P^* is odd, then $P_2 > P_1$ if $\mu < \sigma$, and $P_2 < P_1$ otherwise. This follows from monotonicity of the map on each subinterval L, M, and R. In other words, the ordering rule can be written as

$$\begin{aligned} &E_M R \cdots > E_M M \cdots > E_M L \ldots, \\ &O_M R \cdots < O_M M \cdots < O_M L \ldots, \end{aligned} \tag{6}$$

where $E_M(O_M)$ represents a common leading string with an even (odd) number of letter M.

Generally speaking, the order on the parameter axis does not have a definite relationship with ordering of the words. However, in the antisymmetric map (3), if we denote the parameter value associated with a pattern P by A_P, then the following nice property holds [24].

$$\text{If } P_1 < P_2, \text{ then } A_{P_1} < A_{P_2}, \text{ and vice versa.} \tag{7}$$

This property can be partially verified by inspecting Table 1, where all admissible periodic patterns of period 7 and less as well as their corresponding parameter values are listed. We will refer to these values when studying the Lorenz equations in the next section.

It is important to note that the ordering of these sequences does not depend on the particular model. It is universal for all mappings with two critical points and the antisymmetric property. Of course, the parameter values in Table 1 do depend on the mapping (3) and may be determined by using the word-lifting technique [25]. Therefore, following Metropolis *et al.* [26], we shall call this ordering a U-sequence of symbolic sequences.

A symbolic sequence is called admissible, if it may be produced by the mapping at some parameter A and initial value x_0. Put in other words, an admissible symbolic sequence corresponds to a real orbit of the mapping. Obviously, not every word, made of L, $\bar{C}$, M, C, and R, is admissible.

For a pattern P we denote by $\mathcal{L}(P)$ the set of all subsequences of P that immediately follow one or another letter L in P, i.e.

Table 1. Asymmetric superstable periodic in the antisymmetric cubic map. An asterisk denotes a symmetry-broken orbit

No.	Period	Word	A	No.	Period	Word	A
1	2*	R	3.121 320 3	26	6	$RRMRR$	3.925 457 6
2	4	RMR	3.262 878 6	27	6	$RRMRM$	3.935 027 1
3	6	$RMRLR$	3.334 024 1	28	5	$RRMR$	3.940 904 4
4	6*	$RMMLM$	3.463 283 4	29	6	$RRMRL$	3.946 411 0
5	6	$RMMLR$	3.528 227 2	30	6	$RRMML$	3.950 472 1
6	4	RMM	3.548 085 8	31	5	$RRMM$	3.955 327 4
7	6	$RMMMR$	3.565 988 0	32	6	$RRMMM$	3.959 701 5
8	6	$RMMMM$	3.591 181 9	33	6	$RRMMR$	3.963 799 8
9	5	$RMMM$	3.615 031 9	34	4	RRM	3.967 540 3
10	5	$RMMR$	3.666 207 0	35	6	$RRMLR$	3.971 091 4
11	3	RM	3.700 315 5	36	6	$RRMLM$	3.974 519 8
12	6	$RMLRM$	3.702 984 9	37	5	$RRML$	3.977 781 6
13	5	$RMLR$	3.733 940 7	38	6*	$RRRLL$	3.981 899 0
14	5	$RMLM$	3.775 383 9	39	5	$RRRL$	3.985 488 5
15	6	$RMLMM$	3.790 908 8	40	6	$RRRLM$	3.987 890 5
16	6	$RMLMR$	3.807 368 9	41	6	$RRRLR$	3.990 027 2
17	4*	RRL	3.839 894 4	42	4	RRR	3.991 930 0
18	6	$RRLMR$	3.861 086 0	43	6	$RRRMR$	3.993 628 0
19	6	$RRLMM$	3.873 461 5	44	6	$RRRMM$	3.995 129 5
20	5	$RRLM$	3.883 586 0	45	5	$RRRM$	3.996 426 9
21	6	$RRLML$	3.893 355 0	46	6	$RRRML$	3.997 523 1
22	6	$RRLRL$	3.898 299 2	47	6	$RRRRL$	3.998 411 7
23	5	$RRLR$	3.906 906 3	48	5	$RRRR$	3.999 107 8
24	6	$RRLRM$	3.914 490 1	49	6	$RRRRM$	3.999 603 7
25	3	RR	3.924 990 7	50	6	$RRRRR$	3.999 900 9

$$\mathscr{L}(P) = \{Y | \forall \text{ possible decompositions } P = XLY\} \tag{8}$$

where X and Y are symbolic patterns made of L, M, and R. Similarly, we define $\mathscr{M}(P)$ and $\mathscr{R}(P)$. Denote by K_g and K_s the symbolic sequences, produced by the first iterate of the maximal point $\bar{C}$ and the minimal point C, respectively. These are the kneading sequences of the map. The antisymmetry of the map yields $K_s = \bar{K}_g$, where the conjugate $\bar{K}_g$ of K_g is obtained by interchanging L and R, but leaving M unchanged. The admissibility conditions for a pattern P can be read off from the shape of the mapping function, shown in Fig. 1.

$$\begin{aligned} \mathscr{L}(P) &< K_g, \\ K_s < \mathscr{M}(P) &< K_g, \\ K_s &< \mathscr{R}(P). \end{aligned} \tag{9}$$

It is easy to check that all the words in Table 1 satisfy these conditions. An example which does not belong to the U-sequence is $P = \bar{C}RMLRC$, for which a member of $\mathscr{L}(P)$, namely, $RC \cdots > K_g = RMLRC \ldots$, thus violating the first condition in (9). We will return to this counter example later.

3. THE SYSTEMATICS OF PERIODIC WINDOWS IN THE LORENZ MODEL

We start by inspecting the bifurcation diagram of the Lorenz equations, obtained by plotting the stationary values of x_i in the Poincaré section Σ against the parameter r. A segment of the bifurcation diagram is shown in Fig. 2. The dark lines and periodic windows in this bifurcation diagram, as well as the symmetry breakings and restorations in it,

suggest the possibility to use a one-dimensional antisymmetric map such as (3) to capture the essential features of the Lorenz equations.

In order to get a feeling of the underlying 'one-dimensional' map, we draw a first return map for x, i.e. $x_{i+1} \sim x_i$ dependence, using the x_i values only from the Poincaré map. Figure 3 shows a periodic orbit at $r = 172.77$ (diamonds), superimposed on a chaotic orbit

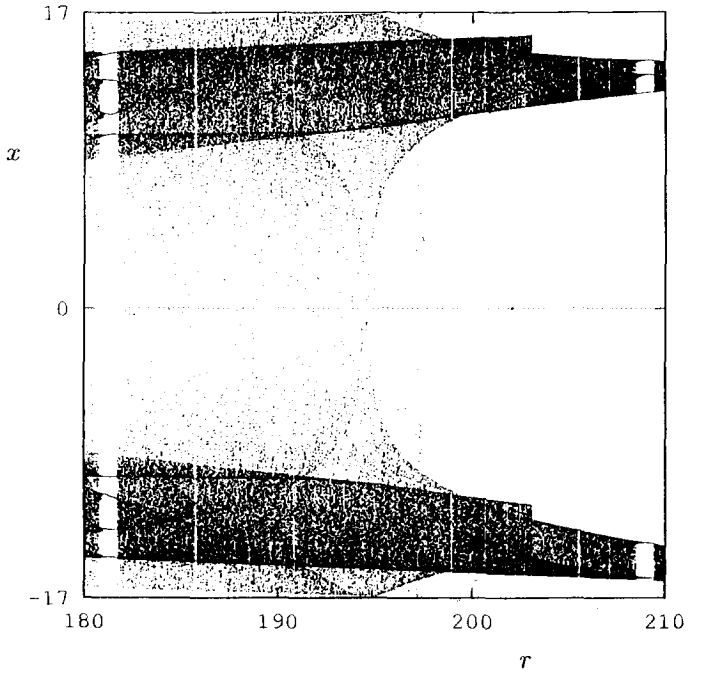

Fig. 2. A bifurcation diagram of the Lorenz equations in the parameter range $r = 180$ to 210.

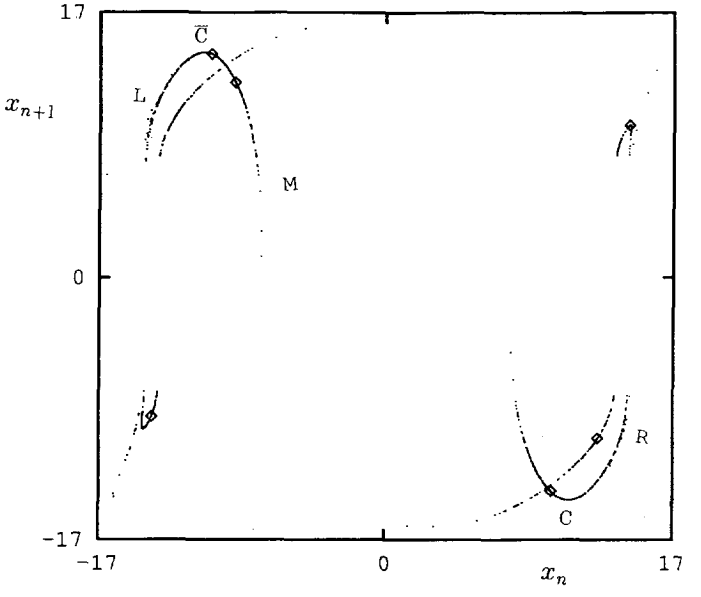

Fig. 3. A periodic 6 orbit at $r = 172.77$ (diamonds), shown on the background of a chaotic trajectory at $r = 172.81$ (dots).

at a near-by parameter $r = 172.81$ (dots). Looking at the periodic points alone, one can imagine them as distributed along a one-dimensional 'cubic' curve. The chaotic attractor, though exhibiting one-dimensional structure, cannot be taken to be a single-valued mapping function due to bending back which leads to self-intersection.

However, for reasons which will become clear in Section 5, we may consider the bent-back part of the attractor as a continuation of the curve before the bend, thus determining two critical points $\bar{C}$ and C, as well as the 'monotone' branches L, M, and R, as shown in Fig. 3. From the symbol assignment at $r = 172.81$, the symbolic sequence for the period 6 orbit at a near-by parameter $r = 172.77$ is derived to be $(RMLMRR)^{\infty}$.

In practice, we always determine the symbol assignment for a periodic orbit from that of a closely related chaotic orbit, using two approaches. The first approach looks at the chaotic orbit right before the tangent bifurcation, which gave birth to the periodic orbit in question, as we just described on the example of Fig. 3.

The second approach makes use of the 'semi-attractor' or chaotic transients [27] at the same parameter value as the periodic orbit. Numerically a semi-attractor may be obtained as follows. Take a set of initial points, distributed randomly in the attracting set of the equations (for the Lorenz system this usually means a region with $|x| < 40$, $|y| < 100$, and $|z| < 200$) and iterate a number of times. The first few, say, five interactions are not plotted. The iterations are stopped when the trajectories get close enough to the stable periodic orbits. The semi-attractor, outlined in this way, looks quite similar to a chaotic attractor, obtained at a near-by parameter. Thus the two methods lead to the same word for the periodic orbit. It is clear that the word $(RMLMRR)^{\infty}$ develops into a superstable word $(RMLMR\bar{C})^{\infty}$ by slightly adjusting the parameter r in the right direction. Therefore, we simply denote this periodic window by $RMLMR$. This has been done for other periodic windows as well.

We summarize our results in Table 2, where all periodic windows discovered so far by us and by other authors are listed in descending r order along with their periods, symbolic sequences and locations on the parameter axis. Only primitive periods, i.e. those which do not come from period-doubling, are shown in Table 2, except for a few period-doubled regimes of the first period 2 orbit. In Table 2 'Period' equals the number of points seen in the Poincaré section Σ for a periodic orbit. We also give the parameter A for the corresponding superstable word in the one-dimensional map (3) for later use.

Table 2 clearly shows that all 67 periodic sequences except for one (No. 10) do fit into the cubic scheme. Moreover, the ordering of all these words happens to be exactly the same as that of their one-dimensional counterparts along the increasing A direction. Take, for example, $P_1 = RRLR$ at $r_1 = 114.0$ and $P_2 = RRLRRL$ at $r_2 = 107.613$. In the cubic map (3) $P_2 > P_1$ according to the ordering rule, given in Section 2, and it follows from property (7) that $A_{P_2} > A_{P_1}$. However, in the Lorenz equations we have $r_1 > r_2$. This simply says that the descending r order in the Lorenz equations corresponds to increasing A order in the cubic map (3). Therefore, parameter r in the Lorenz model is, in a sense, opposite to the parameter A in the cubic map.

The only non-cubic word left in Table 2, namely, the word coming from the symmetric $\bar{C}RMLRC$ at $r = 191.982 - 191.985$, does not satisfy the admissibility conditions of the cubic map (3). We have mentioned this at the end of Section 2. This fact is not surprising, as the return maps of the Lorenz equations are not one-dimensional. We will return to the reason for the appearance of such words in Section 5.2.

Now we are in a position to say that apart from one exception the skeleton of the systematics of periodic windows obeys the 'cubic' law, or put in other words, symbolic dynamics underlying the global periodic structure of the Lorenz equations appears to be essentially the same as that for the cubic map for most of the parameters. To understand

Table 2. Periodic windows for the Lorenz equations. All of them can be fit into the 'cubic' scheme except for No. 10. An asterisk denotes a symmetry-broken orbit; the original symmetric orbit is indicated in parentheses

No.	Period	Word	A	r range
1	2*	$R\ (\bar{C}C)$	3.121 320	314–229.42
	4	RMR	3.262 879	229.42–218.3
	8	$RMRLRMR$	3.293 843	218.3–216.0
	16	$RMRLRMRMRMRLRMR$	3.300 475	216.0–215.5
2	24	$RMRLRMRMRMRLRMRLRMRLRMR$	3.303 736	215.08–215.07
3	12	$RMRLRMRMRMR$	3.309 068	214.06–213.99
4	6	$RMRLR$	3.334 024	209.45–209.06
5	10	$RMRLRLRMR$	3.344 538	207.12–207.106
6	8	$RMRLRLR$	3.352 641	206.528–205.486
7	10	$RMRLRLRLR$	3.358 220	204.123–2.04.116
8	14*	$RMRLRLRLMLRLR(\bar{C}RMRLRLC)$	3.373 058	200.665–200.638
9	10*	$RMRLMLMLR(\bar{C}RMRLC)$	3.394 393	198.99–198.97
10	10*	$RMLRMLMRL(\bar{C}RMLRC)$	not cubic	191.985–191.982
11	5	$RMLR$	3.733 941	190.81–190.80
12	7	$RMLRLR$	3.739 312	189.561–189.559
13	9	$RMLRLRLR$	3.740 172	188.865–188.863
14	16*	$RMLRLRLMLMRLRLR(\bar{C}RMLRLRLC)$	3.740 750	187.25–187.248
15	12*	$RMLRLMLMRLR(\bar{C}RMLRLC)$	3.742 852	185.80–185.74
16	8*	$RMLMLMR(\bar{C}RMLC)$	3.755 828	181.65–181.12
17	10	$RMLMLMLMR$	3.767 426	178.074 5
18	12*	$RMLMLRLMRMR(\bar{C}RMLMLC)$	3.767 734	177.81–177.78
19	6	$RMLMR$	3.790 909	172.797–172.758
20	16*	$RMLMRMLMLMRMLMR(\bar{C}RMLMRMLC)$	3.819 041	169.902
21	10	$RMLMRMLMR$	3.823 171	168.58
22	4*	$RRL(\bar{C}RC)$	3.839 895	166.01–146.2
23	12	$RRLMRRLLRRL$	3.844 115	146–145.94
24	20*	$RRLMRRLLRMLLRMLLRRL$ $(\bar{C}RRLMRRLLRC)$	3.845 424	144.38–144.35
25	12*	$RRLMRMLLRML(\bar{C}RRLMRC)$	3.846 750	143.442–143.322
26	6	$RRLML$	3.893 355	136.818–136.79
27	10	$RRLMLLRRL$	3.893 743	136.21
28	16*	$RRLMLLRMLLRMRRL(\bar{C}RRLMLLRC)$	3.893 849	135.485–135.465
29	8*	$RRLRLLR(\bar{C}RRLC)$	3.895 900	133.2–132.06
30	16*	$RRLRLLRRLLRLRRL(\bar{C}RRLRLLRC)$	3.897 809	129.148–129.127
31	6	$RRLRL$	3.898 299	126.445–126.41
32	12*	$RRLRLRLLRLR(\bar{C}RRLRLC)$	3.903 069	123.63–123.56
33	8	$RRLRLRL$	3.903 380	121.689–121.687
34	7	$RRLRLR$	3.904 451	118.134–118.128
35	14*	$RRLRLRMLLRLRL(\bar{C}RRLRLRC)$	3.906 043	116.925–116.91
36	5	$RRLR$	3.906 906	114.01–113.9
37	10*	$RRLRRLLRL(\bar{C}RRLRC)$	3.918 416	110.70–110.57
38	7	$RRLRRL$	3.919 481	107.625–107.618
49	14*	$RRLRRLMLLRLLR(\bar{C}RRLRRLC)$	3.921 505	106.757–106.746
40	8	$RRLRRLR$	3.922 810	104.185
41	16*	$RRLRRLRRLLRLLRL(\bar{C}RRLRRLRC)$	3.923 422	103.636–103.632
42	3	RR	3.924 991	100.07–99.93
43	9	$RRMRRLRR$	3.925 809	99.285–99.275
44	12*	$RRMLLMLLMRR(\bar{C}RRMLLC)$	3.979 410	94.554–94.542
45	6*	$RRRLL(\bar{C}RRC)$	3.981 899	93.20–92.16
46	12*	$RRRLLMLLLRR(\bar{C}RRRLLC)$	3.984 133	90.20–90.163
47	14*	$RRRLLRRLLLRRL(\bar{C}RRRLLRC)$	3.985 072	85.987–85.986
48	5	$RRRL$	3.985 489	83.39–83.36
49	10*	$RRRLMLLLR(\bar{C}RRRLC)$	3.988 987	82.095–82.040
50	12*	$RRRLRRLLLRL(\bar{C}RRRLRC)$	3.991 025	76.713–76.310
51	14*	$RRRLRRMLLLRLL(\bar{C}RRRLRRC)$	3.991 706	73.457
52	4	RRR	3.991 930	71.52–71.41
53	8*	$RRRRLLL(\bar{C}RRRC)$	3.997 993	69.839–69.724
54	6	$RRRRL$	3.998 412	64.898–64.895
55	12*	$RRRRLRLLLLR(\bar{C}RRRRLC)$	3.998 785	64.574–64.572
56	7	$RRRRLR$	3.998 898	62.069

continued

Table 2.—*continued*

No.	Period	Word	A	r range
57	14*	$RRRRLRRLLLLRL(\bar{C}RRRRLRC)$	3.999006	61.928
58	5	$RRRR$	3.999108	59.255–59.242
59	10*	$RRRRRLLLL(\bar{C}RRRRC)$	3.999777	58.715–58.700
60	7	$RRRRRL$	3.999824	55.787
61	14*	$RRRRRLRLLLLLR(\bar{C}RRRRRLC)$	3.999865	55.675
62	6	$RRRRR$	3.999901	52.459–52.455
63	12*	$RRRRRLLLLL(\bar{C}RRRRRC)$	3.999975	52.245–52.248
64	8	$RRRRRRL$	3.9999804	50.3240–50.3038
65	7	$RRRRRR$	3.9999889	48.1194–48.1181
66	14*	$RRRRRRRLLLLLL(\bar{C}RRRRRRC)$	3.9999972	48.0271–48.0259
67	9	$RRRRRRRL$	3.9999978	46.6683

the reasons, a two-dimensional representation of symbolic dynamics for the two-dimensional map F in Σ is needed. We will continue this discussion in Section 5.2.

Before ending this section, we compare briefly our symbols with Sparrow's in [3]. Our periodic orbit R^n corresponds to $x^n y$ in Sparrow's notation; a symmetric orbit $R^{n-1}\ L^{n-1}$ corresponds to $x^n y^n$. The letter M may represent either x or y. Using the symbolic system of Sparrow, sometimes one can not tell whether a periodic orbit is symmetric or asymmmetric from the word. With one additional letter, it is possible to explore more subtle properties such as ordering of symbolic sequences and symmetry breakings. In fact, Sparrow was not concerned with the construction of a symbolic dynamics with its ordering rules, admissibility conditions and other consequences.

4. SYMBOLIC DYNAMICS OF A TWO-DIMENSIONAL ANTISYMMETRIC CUBIC MAP

In order to prepare for the study of the Lorenz equations, we consider a two-dimensional antisymmetric cubic map [28]:

$$\begin{aligned} x_{n+1} &= Ax_n^3 + (1 - A)x_n + by_n, \\ y_{n+1} &= x_n, \end{aligned} \tag{10}$$

and its symbolic dynamics.

It is well-known that a good partition is crucial for the construction of symbolic dynamics. In one-dimensional maps the generating partitions are determined by critical points. For two-dimensional maps, in order to partition the phase space one-dimensional curves must be used. For the Hénon map, P. Grassberger and H. Kantz conjectured that the line, obtained by connecting all 'primary' tangencies between the stable and unstable manifolds, leads to a generating partition [9]. A natural extension of Grassberger and Kantz's idea is to invoke tangencies between the most stable manifold (MSM) and the backward most stable manifold (BMSM) [29, 30]. A MSM is a submanifold in the basin of an attractor such that all the points on this submanifold will converge to a single point with the highest possible exponential rate (i.e. the most negative Lyapunov exponent of the attractor). Analogously, a BMSM is a submanifold in the basin of an attractor, on which all points, iterated backward, will converge to a single point with the highest possible exponential rate.

If one point of a MSM falls on a stable manifold of a saddle (or periodic orbit), this MSM coincides with the stable manifold of the saddle. All stable manifolds of saddles and periodic orbits form an invariant subset of MSM's and all unstable manifolds of saddles and periodic orbits form an invariant subset of BMSM's. Consequently, all 'primary'

tangencies between stable and unstable manifolds is a subset of the 'primary' tangency set between MSM's and BMSM's. Then the partition can be defined as the 'primary' tangency set between MSM's and BMSM's. The Grassberger–Kantz construction works well when the knowledge of partitions on the attractor is enough; when it comes to dealing with partitions in the whole space, not only on the attractor, the above extension is useful.

Numerically, MSM and BMSM are easily calculable for two-dimensional maps. For ODE's like the Lorenz equations, usually it is rather difficult to calculate the tangencies between the stable and unstable manifolds in the Poincaré sections, but the MSM may be easier to obtain as we will see in the next section.

For the two-dimensional antisymmetric cubic map (10), the generation partition should be a ternary one. To construct this ternary partition, we begin with the extremely dissipative case when $b \to 0$. In this case the MSM's are just straight lines with $x =$ constant, except for $x = \pm C$, which are the turning points. Here $C = \sqrt{(A-1)/3A}$, and $x = \pm C$ are the two critical points of the one-dimensional cubic map (3).

In Fig. 4 we show part of the MSM's and BMSM's together with the attractor of the map (10) at $a = 3.4$ and $b = 0.001$. When $b \to 0$ the straight lines $y = \pm C$ go through a set of tangencies between MSM's and BMSM's, while other tangencies, seen at $x = \pm C$ are their pre-images. The line $y = C$ is denoted by $C\bullet$ and $y = -C$ by $\bar{C}\bullet$, both being partition lines in this limit. As b increases gradually, we can trace how the set of tangencies deviates from the lines $y = \pm C$. Figure 5 shows the situation at $a = 3.4$, $b = 0.25$. The heavy lines are the unstable manifolds which outline the attractor. The thin lines are part of the MSM's. The dotted line is the partition line $C\bullet$ (the undrawn $\bar{C}\bullet$ is antisymmetric to $C\bullet$), which is obtained by connecting the tangent points between MSM's and BMSM's. As expected, $C\bullet$ and $\bar{C}\bullet$ split the two-dimensional phase space into three regions.

It seems that all the tangencies of map (10) are images or pre-images of the set of

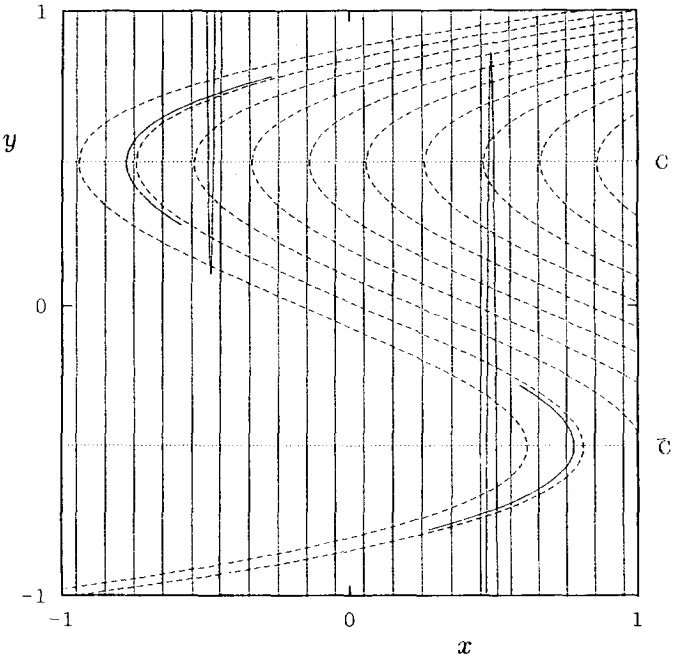

Fig. 4. The most stable manifolds (thin lines), the backward most stable manifolds (dashed lines), and the attractor (solid lines) for the two-dimensional antisymmetric cubic map (10) at $a = 3.4$ and $b = 0.001$. The dotted lines indicate $\bar{C}$ and C, which are formed by tangencies between MSM's and BMSM's. As b approaches 0, the MSM's become vertical straight lines except for segments near the turning points at $x = \pm C$.

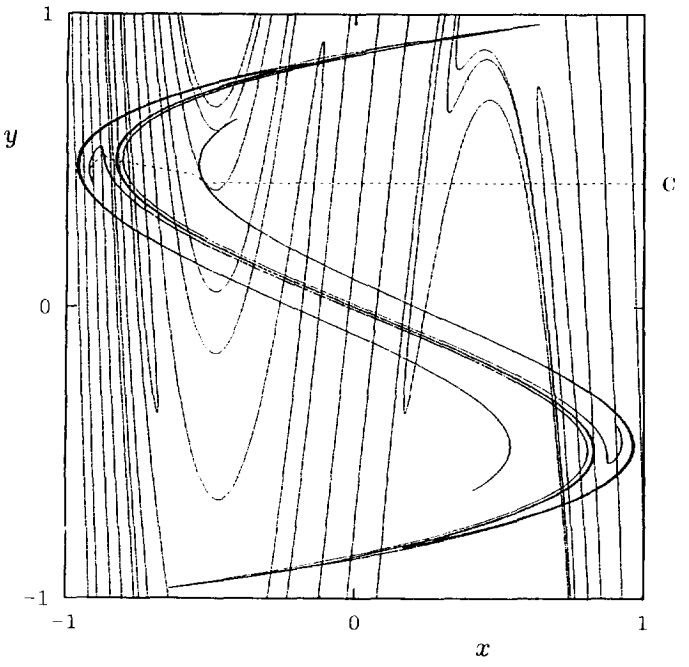

Fig. 5. The MSM's and unstable manifolds for the 2D antisymmetric cubic map (10) at $a = 3.4$ and $b = 0.25$. The heavy lines show the unstable manifolds which outline the attractor. The thin lines are part of the MSM's. The dashed line is the partition line C, obtained by connecting the 'primary' tangencies between MSM's and BMSM's. The other partition line $\bar{C}$ has not been drawn.

tangencies coming from $y = \pm C$ [9]. In this paper, we call this set of tangencies the 'primary' set and the tangencies on this set the 'primary' tangencies. These 'primary' tangencies are consistent with the 'principal' tangent points at which the sum of the curvatures of both stable and unstable manifolds is smaller than any of its images and pre-images, as proposed by Grassberger *et al.* [11].

Now we can construct the symbolic dynamics for map (10) explicitly. Borrowing notations from the one-dimensional antisymmetric cubic map (3), we assign a letter R, M, and L, to the region above C, the region between C and $\bar{C}$, and the region below $\bar{C}$ (see Fig. 5), respectively. An initial point (x_0, y_0) generates a symbolic sequence by iterating the map (10):

$$\cdots s_{\bar{m}} \cdots s_{\bar{1}} s_{\bar{0}} \bullet s_0 s_1 s_2 \cdots s_n \ldots,$$

where s_n denotes the x-symbol of the nth image, $s_{\bar{m}}$ the y-symbol of the $\bar{m}$th preimage, each being one of the five letters R, C, M, $\bar{C}$, and L. The solid dot indicates the 'present' position, which divides the bi-infinite sequence into two semi-infinite ones: the forward symbolic sequence (FSS)

$$\bullet s_0 s_1 s_2 \cdots s_n \cdots$$

and the backward symbolic sequence (BSS)

$$\cdots s_{\bar{m}} \cdots s_{\bar{1}} s_{\bar{0}} \bullet.$$

In this dissipative map, a FSS may correspond to many points in the phase space. These points form a subspace, which is called a forward foliation of the phase space. Similarly, a BSS may correspond to a backward foliation of the phase space [13]. The forward and

backward foliations provide the means to partition the two-dimensional phase space by one-dimensional curves. On each set of these curves the dynamics corresponds to a one-dimensional map. The original two-dimensional map is decomposed into two coupled one-dimensional maps. Thus a substantial part of symbolic dynamics of one-dimensional maps may be transplanted to the two-dimensional case.

In fact, the forward and backward foliations are part of the MSM's and BMSM's. Since all the points on an MSM will converge to a single point, all the points in phase space sharing the same forward sequence must fall on the same MSM. Analogously, all the points in phase space sharing the same backward sequence must fall on the same BMSM. Thus the MSM's and BMSM's provide a way to trace the points with the same forward or backward symbolic sequence in the phase space. Each backward foliation is cut by many forward foliations. All points on a backward foliation share the same backward symbolic sequence. The forward symbolic sequences on one and the same backward foliation are different; they correspond to the FSS of the one-dimensional map (3). Assuming that the ordering rules of the FSS on a backward foliation are the same as that for the one-dimensional limit (3), we have

$$\begin{aligned} &\bullet E_M R \cdots > \bullet E_M M \cdots > \bullet E_M L \ldots, \\ &\bullet O_M R \cdots < \bullet O_M M \cdots < \bullet O_M L \ldots, \end{aligned} \tag{11}$$

where E_M (O_M) represents the common leading string, containing an even (odd) number of letter M. According to these rules, the greatest FSS is $\bullet R^\infty$, while the smallest is $\bullet L^\infty$.

Analogously, each forward foliation is cut by many backward foliations and corresponds to another one-dimensional map. The ordering rules of the BSS on a forward foliation are defined as

$$\begin{aligned} &\cdots R E_{LR}\bullet > \cdots M E_{LR}\bullet > \cdots L E_{LR}\bullet, \\ &\cdots R O_{LR}\bullet < \cdots M O_{LR}\bullet < \cdots L O_{LR}\bullet. \end{aligned} \tag{12}$$

The notation E_{LR} (O_{LR}) now represents the common leading string with the total number of letters L and/or R being even (odd). The greatest BSS is $(LR)^\infty\bullet$, and the smallest is $(RL)^\infty\bullet$.

In Table 3, we list the maximal and minimal FSS or BSS with a leading R, M, or L.

These ordering rules for FSS and BSS have a clear geometrical background. For each one-dimensional forward (or backward) foliation which is topologically equal to a straight line segment, we can always define the order referring to the natural order on a straight line and then the ordering rules can be defined as for one-dimensional maps. Numerically we find the ordering rules for the forward and backward foliation is just the same as that of the one-dimensional map (3).

Recently, we have considered a piecewise linear two-dimensional antisymmetric map

$$\begin{aligned} x_{n+1} &= \theta_n + \epsilon_n x_n + b y_n, \\ y_{n+1} &= x_n, \end{aligned} \tag{13}$$

Table 3. The maximal and minimal FSS and BSS with a leading R, M or L

	FSS			BSS		
Leading letter	L	M	R	L	M	R
Minimal word	$\bullet L^\infty$	$\bullet MR^\infty$	$\bullet RL^\infty$	$(RL)^\infty\bullet$	$(RL)^\infty M\bullet$	$(LR)^\infty R\bullet$
Maximal word	$\bullet LR^\infty$	$\bullet ML^\infty$	$\bullet R^\infty$	$(RL)^\infty L\bullet$	$(LR)^\infty L\bullet$	$(LR)^\infty\bullet$

where

$$\begin{cases} \theta_n = -\dfrac{c+d}{1-c}\,\mathrm{sgn}(x_n), & \epsilon_n = \dfrac{1+d}{1-c}, & C < |x_n| \leqslant 1, \\ \theta_n = 0, & \epsilon_n = -\dfrac{d}{c}, & |x_n| \leqslant C. \end{cases}$$

In these equations c, d, b are parameters with their values all between 0 and 1, and $\mathrm{sgn}(x_n)$ denotes the sign of x_n.

$$\mathrm{sgn}(x) = \begin{cases} 1 \\ 0 \\ -1 \end{cases} \quad \text{if} \quad \begin{cases} x > 0, \\ x = 0, \\ x < 0. \end{cases}$$

This map possesses the same antisymmetry as map (10); both maps (10) and (13) consist of three monotonic branches when b approaches 0. For this piecewise linear map, we can define an ordering rule for the forward and backward sequences by referring to left or right, up or down of the corresponding foliation explicitly. These turn out to be the same as the ordering rule defined above for map (10).

It is more convenient to introduce a metric representation [10] for the FSS and BSS. We define a real number α for the FSS and a number β for BSS as follows:

$$\alpha = \sum_{i=1}^{\infty} \mu_i 3^{-i}, \qquad \beta = \sum_{i=1}^{\infty} \nu_i 3^{-i}, \tag{14}$$

where

$$\mu_i = \begin{cases} 0 \\ 1 \\ 2 \end{cases} \text{ for } \prod_{k=1}^{i} p_k^F = 1 \text{ and } s_i = \begin{cases} L, \\ M, \\ R, \end{cases} \text{ or for } \prod_{k=1}^{i} p_k^F = -1 \text{ and } s_i = \begin{cases} R, \\ M, \\ L, \end{cases}$$

$$\nu_i = \begin{cases} 0 \\ 1 \\ 2 \end{cases} \text{ for } \prod_{\bar{k}=1}^{i} p_{\bar{k}}^B = 1 \text{ and } s_{\bar{i}} = \begin{cases} L, \\ M, \\ R, \end{cases} \text{ or for } \prod_{\bar{k}=1}^{i} p_{\bar{k}}^B = -1 \text{ and } s_{\bar{i}} = \begin{cases} R, \\ M, \\ L. \end{cases}$$

Here p_k^F is the parity of the kth letter in a FSS and $p_{\bar{k}}^B$—that of the $\bar{k}$th letter in a BSS:

$$p_k^F = \begin{cases} 1 \\ -1 \end{cases} \quad \text{if} \quad \begin{cases} s_k = R \text{ or } L, \\ s_k = M, \end{cases} \qquad \text{and} \qquad p_{\bar{k}}^B = \begin{cases} 1 \\ -1 \end{cases} \quad \text{if} \quad \begin{cases} s_{\bar{k}} = M, \\ s_{\bar{k}} = R \text{ or } L. \end{cases}$$

According to these definitions, we have

$$\begin{aligned} \alpha(\bullet R^{\infty}) &= \beta((LR)^{\infty}\bullet) = 1, \\ \alpha(\bullet RL^{\infty}) &= \beta((LR)^{\infty}R\bullet) = 2/3, \\ \alpha(\bullet ML^{\infty}) &= \beta((LR)^{\infty}M\bullet) = 2/3, \\ \alpha(\bullet MR^{\infty}) &= \beta((RL)^{\infty}M\bullet) = 1/3, \\ \alpha(\bullet LR^{\infty}) &= \beta((RL)^{\infty}L\bullet) = 1/3, \\ \alpha(\bullet L^{\infty}) &= \beta((RL)^{\infty}\bullet) = 0. \end{aligned} \tag{15}$$

In this metric representation, any semi-infinite sequence corresponds to a real number between zero and one. The order for the forward words and the backward words becomes

the natural order for α and β, respectively. A bi-infinite symbolic sequence now corresponds to a point in a unit square of the (α, β)-plane, which is called the symbolic plane. In this plane, backward and forward foliations become vertical and horizontal lines.

So far we have not mentioned $\bullet\bar{C}$ and $\bullet C$. The metric representation for $\bullet C$ lies between $\bullet M$ and $\bullet R$. Since $\bullet M < \bullet R$, we define $\bullet M < \bullet C < \bullet R$. Now $\bullet RL^{\infty}$ is the minimal word for all FSS with a leading R and $\bullet ML^{\infty}$ is the maximal word for all FSS with a leading M, see Table 3. Since $\alpha(\bullet RL^{\infty}) = \alpha(\bullet ML^{\infty}) = 2/3$ and $\bullet C$ is included in between $\bullet RL^{\infty}$ and $\bullet ML^{\infty}$, it follows that $\alpha(\bullet C)$ must equal to 2/3. Therefore, if there is a C in a FSS, we may replace it by either ML^{∞} or RL^{∞}. Analogously, $\bullet L < \bullet\bar{C} < \bullet M$ and $\bullet\bar{C}$ is included in between $\bullet LR^{\infty}$ and $\bullet MR^{\infty}$, therefore $\alpha(\bullet\bar{C}) = 1/3$. As long as a $\bar{C}$ appears in a FSS, it may be replaced by either LR^{∞} or MR^{∞}. In a BSS, a letter C may be substituted by either $(LR)^{\infty}R$ or $(LR)^{\infty}M$, and a $\bar{C}$ by either $(RL)^{\infty}M$ or $(RL)^{\infty}L$.

Having defined the ordering rules for FSS on each backward foliation and that for BSS on each forward foliation, we are in a position to formulate the admissibility conditions for symbolic sequences. Consider a forward foliation $\bullet J$, which crosses the partition C at P. Denoting the backward symbolic sequence from P by $IC\bullet$, the two symbolic sequences from the points, infinitesimally shifted from P, are $IR\bullet$ and $IL\bullet$. From our knowledge of the one-dimensional map (3), there are no other words admissible between the words $IR\bullet$ and $IL\bullet$, except for the word $IC\bullet$. In the symbolic plane, these forbidden words correspond to a vertical line segment from $[\alpha(\bullet J), \beta(IL\bullet)]$ to $[\alpha(\bullet J), \beta(IR\bullet)]$. Consider all the points on the lines $C\bullet$ and $\bar{C}\bullet$ one by one, we can get a series of such forbidden vertical line segments in the symbolic plane. All the forbidden vertical lines form a forbidden area, called the fundamental forbidden zone (FFZ) [13].

In Fig. 6, we present the the FFZ (empty box) for the map (10) for parameters $a = 3.4$ and $b = 0.25$, where 800 points of $C\bullet$ and $\bar{C}\bullet$ are taken, in which we find the tangent points for the attractor are of minor importance, and at each point forward and backward

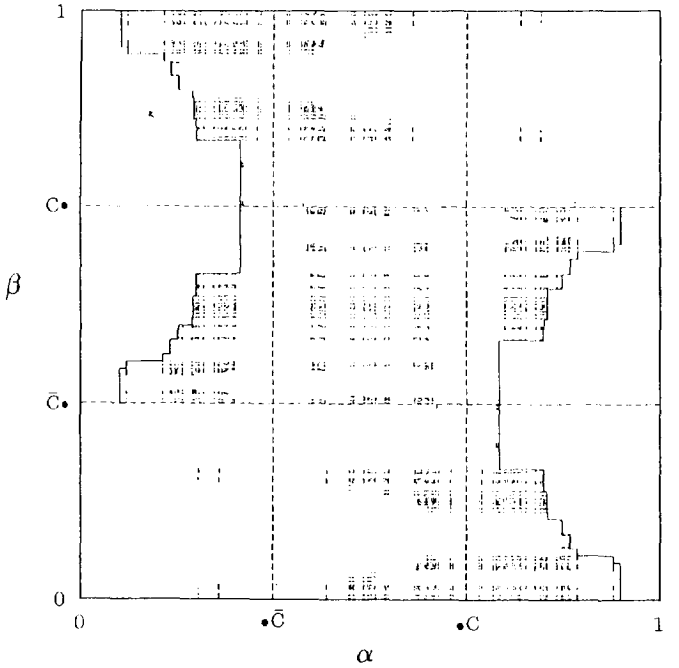

Fig. 6. 60000 points, generated by real orbits in the 2D antisymmetric map at $a = 3.4$ and $b = 0.25$, are shown together with the fundamental forbidden zone (empty part) in the symbolic plane.

sequences of length 20 are generated. The solid lines are the boarder between admissible and inadmissible words in the symbolic plane (the 'pruning front' according to [10]). Owing to the antisymmetry of the map the pruning front is symmetric with respect to the center (1/2, 1/2) of the symbolic plane.

In a given bi-infinite symbolic sequence $\cdots s_{\bar{1}}s_{\bar{0}} \bullet s_0 s_1 \ldots$, after k forward or backward iterations, the 'present' dot $\bullet$ shifts to the right or to the left by k symbols. If the unshifted word corresponds to a real orbit of the map (10), all its shifts must never fall into the FFZ. This statement may be taken as the admissibility condition for a word: a bi-infinite symbolic sequence is admissible if and only if all its shifts never fall inside the FFZ.

In addition, from the antisymmetry of the map (10), it is easy to see that if a word P is admissible (forbidden), so is its conjugate $\bar{P}$; the conjugate $\bar{P}$ is obtained from P by interchanging L and R, while leaving M unchanged.

To check the above admissibility conditions, we picked up 60,000 points randomly in the region $x \in [-1, 1]$ and $y \in [-1, 1]$ and calculated the (α, β)-values for orbits starting from these points which are also shown in Fig. 6. Indeed, no points are contained in the FFZ although many points are very close to the pruning front.

From the admissibility conditions we can enumerate all the admissible words. We list all the primitive admissible words, i.e. those that are not repetitions of a shorter string, up to period 8 in Table 4.

5. LORENZ EQUATIONS IN LIGHT OF SYMBOLIC DYNAMICS OF TWO-DIMENSIONAL MAPS

Now we come to the main body of this pape. Our basic goal is to construct a symbolic dynamics for the Lorenz map F. Although it is approximate, it works well for all practical purposes for most of the parameter r range. This is done in Section 5.2, after introducing the extended geometric Lorenz map G in Section 5.1. In Section 5.3 we show how to predict new periodic orbits in the Lorenz equations by using the symbolic dynamics. The last Section 5.4 furnishes a qualitative discussion of the relation between the extended geometric Lorenz map and the geometric Lorenz attractor.

5.1. *The extended geometric Lorenz attractor*

Recall our description of the Lorenz map F in Section 1. We take, for example, $r = 110$. In the 'rectangle' Σ contained in the plane $z = r - 1$, the attractor and the most stable

Table 4. Admissible primitive periodic sequences up to period 8 in the 2D map (10) at $a = 3.4$, $b = 0.25$. A letter X stands for L or M. Only non-repeating strings are given and the conjugate words are not listed

Period	Allowed sequence	Period	Allowed sequence
1	*X*	7	*RMMMLRX*
2	*RX*	8	*RRLRMMRX*
4	*RMRL*	8	*RMRLRMRM*
5	*RMMRX*	8	*RMMMRMRX*
6	*RMRLRX*	8	*RMMLRMRX*
6	*RMMMRX*	8	*RMRLRLRX*
6	*RMMLRX*	8	*RMMMRLRX*
7	*RMMRMRX*	8	*RMMMMMRX*
7	*RMMRLRX*	8	*RMMMMLRX*
7	*RMMMMRX*	8	*RMMLRLRX*

manifolds are presented in Fig. 7. Since the eigenvalues of the two equilibrium points q^- and q^+ are complex in this plane, we have to introduce a separating line D to cut the spiraling most stable manifolds as the dotted line shows in Fig. 7.

To derive the extended geometric Lorenz map G in Σ from the actual two-dimensional Lorenz map F, we make the following five additional geometric assumptions.

Assumption 1. The attractor, i.e. the set of accumulation points of the map when $t \to \infty$, is composed of two one-dimensional curves, as shown in Fig. 8. Due to strong dissipation, the attractor for the Lorenz map in Σ has a very narrow width. Its structure, transversal to the one-dimensional curves, can be seen only at greater magnification (cf. Fig. 7). The attractor of the extended geometric Lorenz map G is the extremely dissipative limit of that of the Lorenz map F.

Assumption 2. There exists a set of most stable manifolds in Σ, as shown in Fig. 8. Then almost all the points in the plane will be attracted to the attractor along the most stable manifolds with the rate of the most negative Lyapunov exponent of the attractor. This also opens up the possibility to give a two-dimensional representation of the symbolic dynamics for this map. Since the smallest Lyapunov exponent for the dissipative dynamical system is always negative, the MSM's do exist in Σ for the Lorenz equations.

We emphasize that the MSM's, shown in Fig. 7, are actual numerical results for the Lorenz equations, while those in Fig. 8 are schematic drawings to fix the idea of our extended geometric Lorenz attractor.

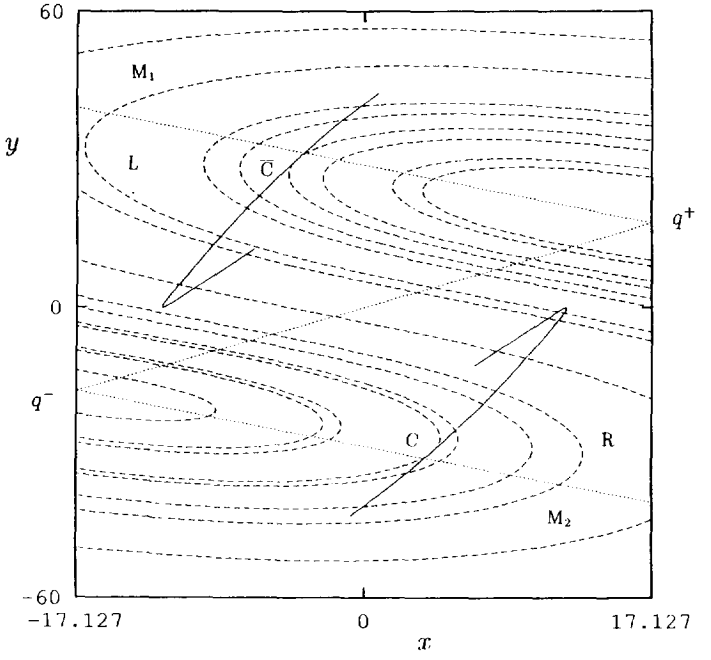

Fig. 7. The MSM's and the attractor of the Lorenz equations at $r = 110$. The heavy lines with hooks are the attractor, which coincides with part of the BMSM's. The dashed lines are part of MSM's. The solid dots, marked by C and $\bar{C}$, are primary tangencies between MSM's and BMSM's. The dotted lines, which represent the ternary partition C and $\bar{C}$, and the separating line D, which connects the two equilibrium points q^- and q^+, divide the phase space into four parts, denoted by L, R, M_1, and M_2.

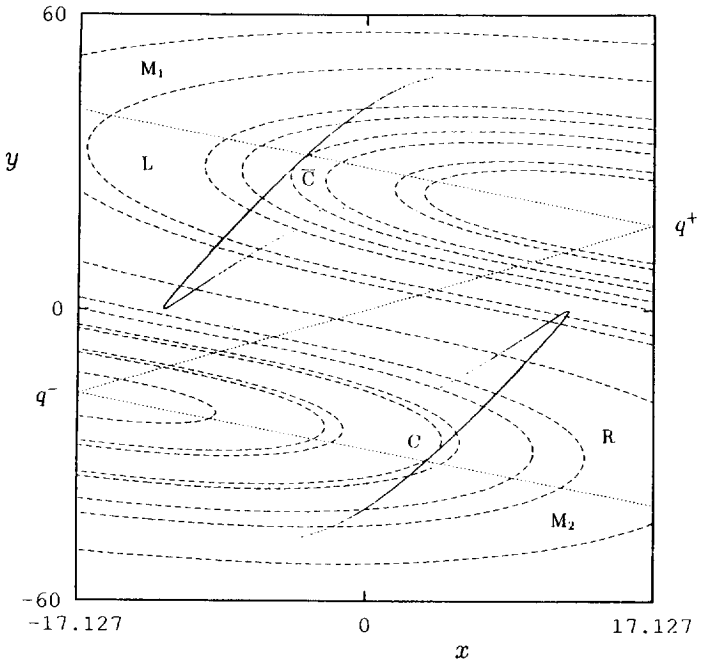

Fig. 8. The MSM's and the attractor for the extended geometric Lorenz map. The lines and points have the same meaning as in Fig. 7.

Assumption 3. There are tangencies between the curves of the attractor and the MSM's. We take $\bar{C}$ and C to be the 'primary' tangent points, as shown in Fig. 8. The ternary partition lines are shown as dashed lines, which are also denoted by $\bar{C}$ and C. It is essential that the partition line goes through the points C and $\bar{C}$. The precise location of partition lines in other parts of the phase plane may be determined by tangent points between MSM's and BMSM's, but is not needed here. Therefore, the dashed lines in Fig. 8 are drawn somewhat arbitrarily when far from $\bar{C}$ and C.

Assumption 4. All points of the interior of Σ do return to Σ and the return map G can be well defined (cf. property (3) below).

Assumption 5. The map G is antisymmetric with respect to the origin $(0, 0)$.

These 'geometric' assumptions can be verified numerically. In Section 5.2, we will give a symbolic description for the actual Lorenz map F. Then we compare the topology of the map F with the geometric map G. We will see, for most of the parameters, the map F can be described by G to very high accuracy.

From the first three assumptions, Σ is divided into four regions by the separating line D and the ternary partition lines $\bar{C}$ and C. We mark them by L, M_1, M_2 and R as shown in Fig. 8. Each region is filled by a family of curves from the MSM's. Introducing a system of coordinates (u, v) on G such that the MSM's are given by $u =$ constant. Here we do not assume the existence of the BMSM's. If the BMSM's exist, they are given by $v =$ constant. Anyway, the attractor can be defined as $v = c$, c being a constant. In fact, the fourth assumption includes two parts: one is the iteration property of u as defined in point (3) below; the other is that all the points in region M_1 will return to the hook in the right branch and all the points in region M_2 to the hook in the left branch of the attractor.

Defining the right one of the two MSM's to be greater and $R > M_2 > M_1 > L$, we can describe the extended geometric Lorenz map analytically as follows.

1. There exists a ternary partition C, $\bar{C}$, and a separating line D to divide the plane Σ into four parts. In each part the curves of MSM are given by u = constant.
2. There exist functions f and g such that G has the form $G(u, v) = (f(u), g(u, v))$ for $u \neq 0$ and $G(-u, -v) = -G(u, v)$.
3. $f'(u) > 0$ in regions R and L; $f'(u) < 0$ in regions M_1 and M_2; $|f'(u)| \to \infty$ as $u \to 0$.

For the attractor of the extended geometric Lorenz map G, $v = c$. The map $G(u, v) = (f(u), g(u, v))$ is completely determined by $f(u)$. In what follows we concentrate on the study of the dynamics of the map $f(u)$.

In Fig. 9 we present a scheme for $f(u)$ which is a one-dimensional map with a discontinuity at $u = 0$. For this one-dimensional map, it is easy to construct the symbolic dynamics explicitly. The ordering rules are

$$\begin{aligned} &E_M R \cdots > E_M M_2 \cdots > E_M M_1 \cdots > E_M L \ldots, \\ &O_M R \cdots < O_M M_2 \cdots < O_M M_1 \cdots < O_M L \ldots, \end{aligned} \tag{16}$$

where E_M (O_M) represents a common leading string with an even (odd) number of letter M_1 and/or M_2. According to these rules, the greatest word is R^∞, while the smallest is L^∞.

This ordering rule provides a criterion to exclude all illegal words.

We denote by K_g and K_s the kneading sequences, i.e. the words coming from the first iterate of the greatest point $\bar{C}$ and that from the smallest point C. The antisymmetry of the map yields $K_s = \bar{K}_g$, $\bar{K}_g$ being the conjugate of K_g, obtained by interchanging L's and R's, but leaving M's unchanged. Analogously, K_D denotes the minimal word iterated from region M_1 and $\bar{K}_D$—the maximal word iterated from region M_2. Using these notations, the

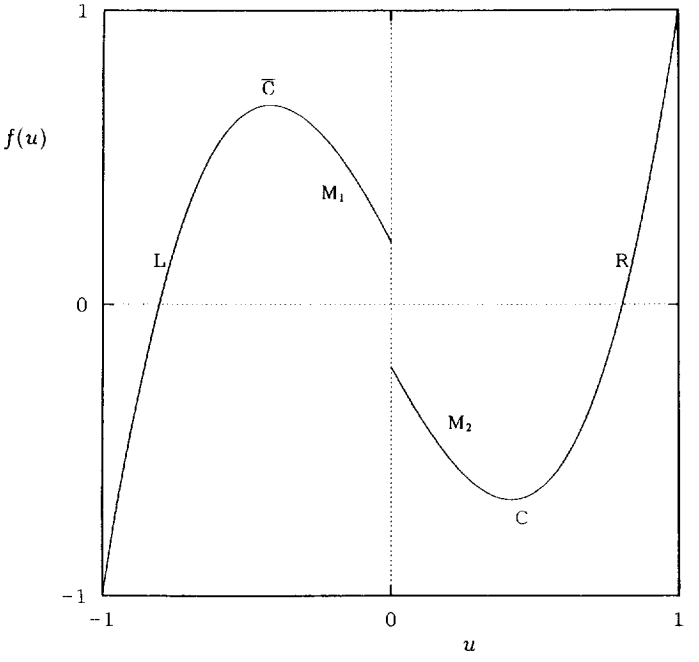

Fig. 9. A sketch of the map $f(u)$. In the figure L, M_1, M_2, and R denote the subintervals, formed by the two critical points C, $\bar{C}$, and the discontinuity point $u = 0$.

admissibility conditions for symbolic sequences in the extended geometric Lorenz map G are formulated as follows: a word P is admissible if all its shifts satisfy the conditions

$$\begin{aligned} \mathscr{L}(P) &< K_g, \\ K_D < \mathscr{M}_1(P) &< K_g, \\ K_s < \mathscr{M}_2(P) &< \bar{K}_D, \\ K_s < \mathscr{R}(P), & \end{aligned} \tag{17}$$

where $\mathscr{L}(P)$, $\mathscr{M}_1(P)$, $\mathscr{M}_2(P)$, and $\mathscr{R}(P)$ are defined in the same way as in (8).

In fact, the symbolic representation of this extended geometric Lorenz map can be constructed by using only three letters. Due to Assumption 4, all points in region M_1 return to the hook in the right branch and all points in region M_2—to the hook in the left branch of the attractor, as shown in Fig. 8. In terms of symbolic dynamics, a letter M_1 will always be followed by a letter R, and a letter M_2 by L. It causes no confusion to mark both M_1 and M_2 by a letter M. Once a substring MR appears, it must be M_1R. Analogously, ML always represents M_2L. In this way, the ordering rule for symbolic sequences in the extended geometric Lorenz map G reduces to that for the one-dimensional antisymmetric map, i.e. (6).

However, the admissibility conditions for map G differs from that for map (3) due to the presence of a discontinuity. A word P is admissible in the extended geometric Lorenz map G if it satisfies the following conditions:

$$\begin{gathered} \mathscr{L}(P) < K_g, \\ K_D < \mathscr{M}(P) < K_g, \quad \text{or} \quad K_s < \mathscr{M}(P) < \bar{K}_D, \\ K_s < \mathscr{R}(P). \end{gathered} \tag{18}$$

In addition, if $K_D > C$ holds, which would imply that no substring MM is admissible.

Now we compare the symbolic dynamics of this extended geometric Lorenz map G with that of the one-dimensional antisymmetric map (3). The ordering rules and admissibility conditions for the one-dimensional antisymmetric cubic map (3) have been given in Section 2, see (6) and (9).

If we ignore the separating line D, i.e. taking $K_D = \bar{K}_D = M^\infty$, the admissibility conditions (18) for the extended geometric Lorenz map G would reduce to (9). Therefore, symbolic sequences in the extended geometric Lorenz map is a subset of that of the one-dimensional antisymmetric cubic map (3). Comparing directly Fig. 9 of map $f(u)$ with Fig. 1 of map (3), we come to the same conclusion.

In the beginning of this section, we have extracted the extended geometric Lorenz map G from the real Lorenz map F in Σ by making a few geometric assumptions. We expect that the behaviour of the map G is topologically similar to that of the map F. We do find that the real Lorenz map F can be described by this extended geometric Lorenz map G for most of the parameter ranges. This will be presented in the next section. In this way, the numerical result of Section 2, namely, periodic windows in the Lorenz equations are well described by the one-dimensional antisymmetric cubic map with only one exception, can be better understood.

5.2. *Symbolic dynamics for the Lorenz map F*

Now we construct the symbolic dynamics for the Lorenz map F explicitly. We take $r = 110$ and $r = 191.99$ as two contrasting examples. Numerical calculation shows that the

$r = 110$ case can be taken as a prototype for the Lorenz map F for most of the parameters except for r close to 191.985, when we encounter the non-cubic word.

The attractor, the most stable manifold, and the separating line D at $r = 110$ have been shown in Fig. 7. A closer examination of the attractor shows that it has a very complicated structure that can not be described as two one-dimensional curves. In Fig. 10, part of the attractor is shown enlarged. Consequently, there are infinitely many primary tangent points in the attractor. According to the definition, given in Section 4, the partition line should go through all these tangent points, which is a subset of tangencies between MSM's and BMSM's of the map F.

The antisymmetry of the map F calls for a ternary partition. In practice, we only determine the partition $\bar{C}$: C can be obtained from the antisymmetry. We record a tangent point if at that point the angle between the tangent vectors of the MSM and the BMSM is smaller than a preset tolerance $\epsilon = 10^{-3}$. From about 100,000 points in the attractor, we obtained 19 such points which are shown in Fig. 10 as crosses. The ternary partition is then determined. As in the extended geometric Lorenz attractor, we label by R the region bounded by D and C, by L the region bounded by D and $\bar{C}$, and by M the regions above $\bar{C}$ and below C. The forward and backward words for these 19 points are then calculated. Taking into account the fact that the map shares the same discrete symmetry as the two-dimensional antisymmetric cubic map (10), the ordering rules for these symbolic sequences are assumed to be the same as for map (10). The metric representation of symbolic sequences is defined by (14). By computing the α and β values for the points on $\bar{C}$, the 'pruning front' and the fundamental forbidden zone (FFZ) are obtained and shown in Fig. 11.

It follows from the discussion of Section 4 that all admissible sequences and their shifts will never fall into the FFZ. To check this condition, the (α, β)-values for 14,162 points in

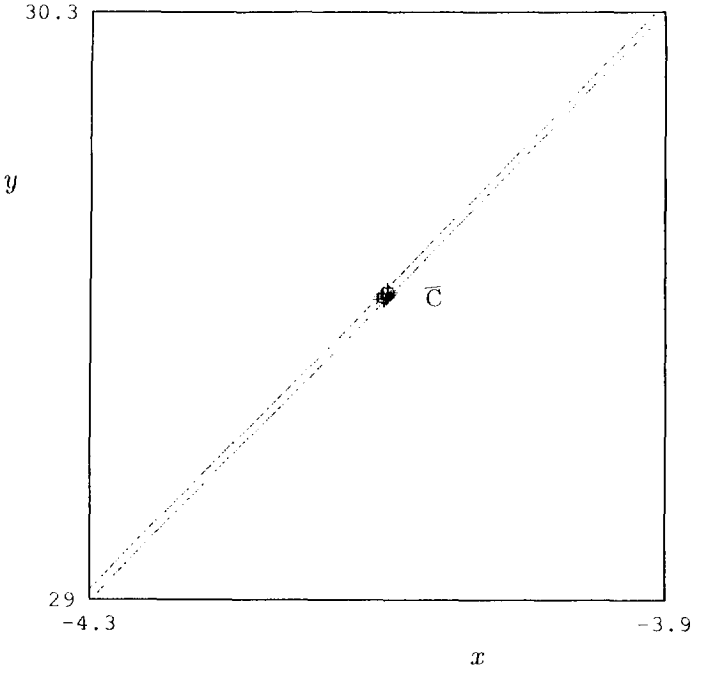

Fig. 10. Part of the attractor around $\bar{C}$ for the Lorenz equations in $\sum$ at $r = 110$. The crosses are primary tangent points.

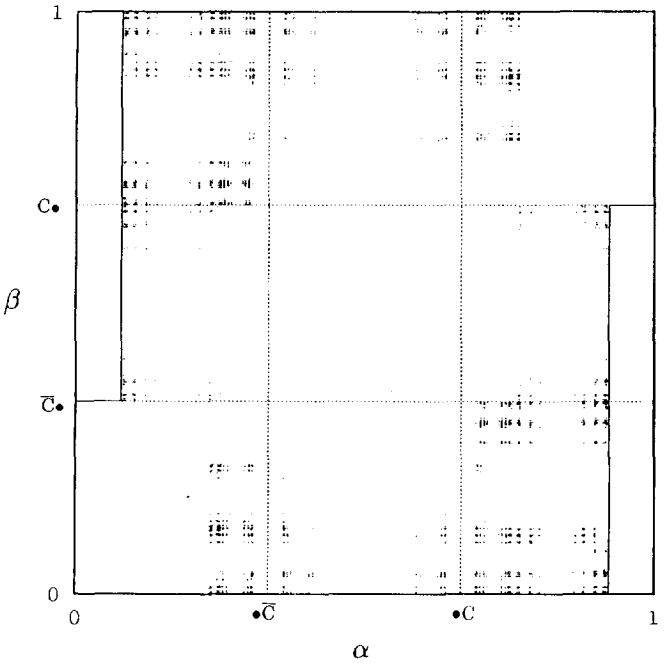

Fig. 11. The symbolic plane of the Lorenz map at $r = 110$. All points represent real orbits. Only one point falls into the FFZ.

the attractor are calculated and shown in Fig. 11. Except for one point, all other points do keep themselves out of the FFZ. The exceptional point will be discussed after we construct the symbolic dynamics for the map F at $r = 191.99$. Therefore, excluding these rare exceptions, we may say that the admissibility condition for a bi-infinite symbolic sequence P of the Lorenz map F at $r = 110$ consists of the fact that its shifts and their conjugates never fall into the FFZ and never satisfy

$$\bar{K}_D < \mathcal{M}(\text{Forw}(P)) < K_D, \tag{19}$$

where Forw(P) represents the forward part of all shifts of P and their conjugates, and K_D is the same as that defined in the extended geometric Lorenz map G, i.e. the maximum word from the topmost point of the left branch in Fig. 8.

Now we compare the symbolic dynamic of the two-dimensional map F with the extended geometric Lorenz map G. Figure 12 is a blow-up of the symbolic plane, i.e. Fig. 11, along the $\beta = 1/3$ line for $\alpha \in [\alpha_{\min}, \alpha_{\max}]$, where $\alpha_{\min} = 0.92215072$ and $\alpha_{\max} = 0.92215080$. This was calculated using all the points on the partition line $\bar{C}$. We can get a sufficient condition for a symbolic sequence of map F to be admissible by only considering its forward sequence: a bi-infinite symbolic sequence is admissible if all α-values of its shifts and their conjugates are never greater than $\alpha_{\min}$ and never satisfy (19); a bi-infinite symbolic sequence is forbidden if one of the α-values of its shifts and their conjugates is greater than $\alpha_{\max}$.

The range for the α values on $\bar{C}$ is $\delta = \alpha_{\max} - \alpha_{\min} = 8{*}10^{-8}$. Since $\log_3 \delta^{-1} = 14.87$, all the first fourteen letters for these forward symbolic sequences turn out to be the same, namely, *RRLRRLLRLRLLRL*. Any unstable periodic orbit with length $n < 15$ can not tell the difference between $\alpha_{\min}$ and $\alpha_{\max}$ [32]. Consequently, the admissibility condition for an unstable periodic orbits with length $n < 15$ is: that a bi-infinite symbolic sequence P is admissible if and only if it satisfies

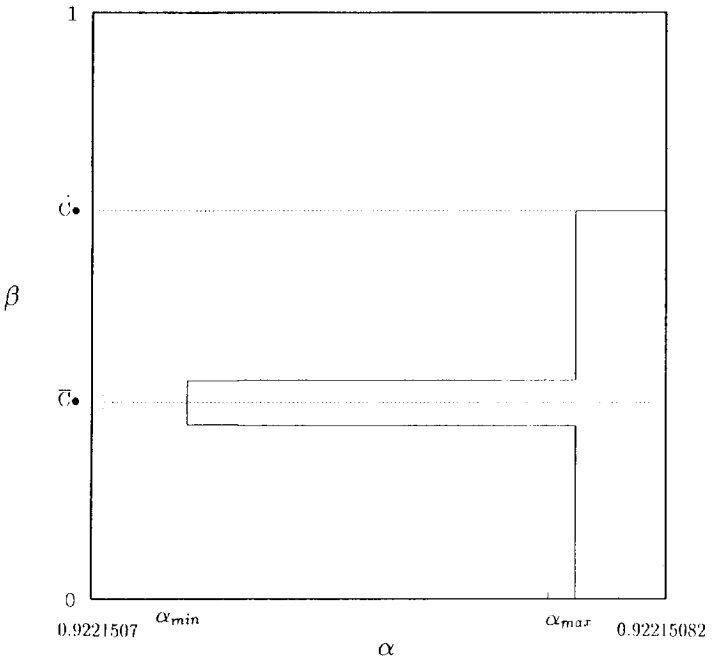

Fig. 12. Blow-up of part of the FFZ, shown in Fig. 11.

$$\begin{gathered} \mathscr{L}(\mathrm{Forw}(P)) < K_g, \\ K_D < \mathscr{M}(\mathrm{Forw}(P)) < K_g), \quad \text{or} \quad K_s < \mathscr{M}(\mathrm{Forw}(P)) < \bar{K}_D, \\ K_s < \mathscr{R}(\mathrm{Forw}(P)). \end{gathered} \tag{20}$$

with $K_g = (RRLRRLLRLRLLRL)^\infty$. This is just the admissibility condition (18) for the extended geometric Lorenz map G. Thus, the topology of the Lorenz map at $r = 110$ is the same as that of the extended geometric Lorenz map G when we only consider periodic orbits with length $n < 15$. The Lorenz map F can be described by the extended geometric Lorenz map G to very high accuracy.

Now we consider the exceptional case when there is a qualitative difference between the Lorenz map F and the extended geometric Lorenz map G. The only such cases occur near $r = 191.99$. The attractor, the most stable manifold, the separating line D, and the ternary partitions $\bar{C}$ and C at $r = 191.99$ are shown in Fig. 13. Unlike the $r = 110$ case, there are primary tangent points in the hooks so that the partition $\bar{C}$ passes through these points. We compute the α and β values for points on the partition line $\bar{C}$, in the same way as we did above.

There are two series of 'pruning' fronts, if we still keep the word 'pruning'. One comes from points on the main branch of the attractor as the case for $r = 110$. This front is shown by the dashed line in Fig. 14. The other comes from the partition points located in the hook; this is shown by the solid line in Fig. 14. In the lower right part of the symbolic plane the second 'pruning' front is located to the right of the first one. The fundamental forbidden zone is defined as the region bounded by this series of 'pruning' fronts, and the lines $\alpha = 1$, $\beta = 0$, and $\beta = 2/3$. A real trajectory and its conjugates will never fall into the FFZ. This has been checked directly by calculating the (α, β) values for 10,582 points in the attractor. These points are also shown in Fig. 14. Indeed, no points fall into the FFZ. It is clear that some points between the first set of 'pruning' front (dashed line) and the

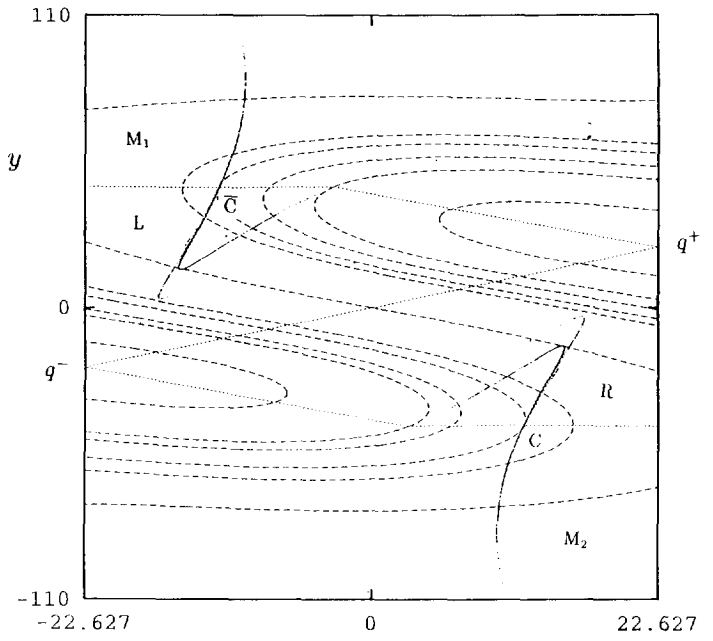

Fig. 13. The MSM's and the attractor of the Lorenz equations in $\sum$ at $r = 191.99$. The lines and points have the same meaning as in Fig. 7.

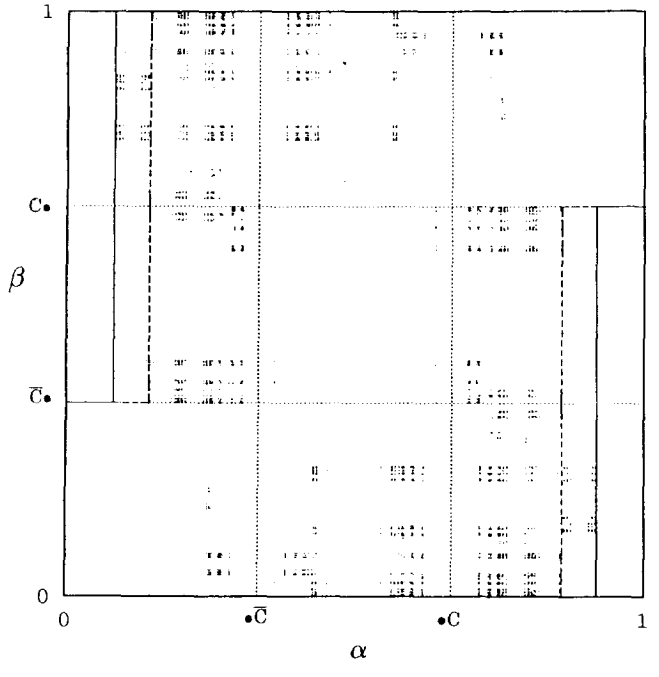

Fig. 14. The symbolic plane of the Lorenz map at $r = 191.99$. All points represent real orbits. The dashed lines show the 'pruning front', determined from partition points on the main branch of the attractor; the solid lines show it from the hook.

second set (solid line) may be forbidden by the first set. Thus, no sufficient admissibility conditions can be formulated.

In this case, the symbolic dynamic is not well constructed since the admissibility conditions can not be well defined. Therefore, the topology of F can not be correctly described by the one-dimensional antisymmetric cubic map (3). By comparing the symbolic dynamics for this case and the $r = 110$ case, it seems that the appearance of the primary tangent points in the hooks accounts for the difference. In fact, though the MSM's of the Lorenz map F can be well constructed and ordered, the BMSM's can not be well defined and ordered which affects the ordering of the backward symbolic sequences. Fortunately, numerical calculation shows that the BMSM's on the main branches of the attractor is ordered rather well. Thus the symbolic dynamics for the Lorenz map F can be well constructed when there are no primary tangent points in the hooks, i.e. when r is far from 191.99.

In fact, primary tangent points do exist in the hooks even for r different from 191.99. In the $r = 110$ case, we did have seen one point which falls into the FFZ (see Fig. 11). However, the probability for a point coming close to these primary tangent points in the hooks is very low and is estimated to be about 1/14,000 at $r = 110$. Consequently, the symbolic dynamics, constructed above, is capable to reflect the topology of the Lorenz map F very well. For other parameters, it can be verified numerically that the probability for a point coming close to primary tangent points in the hooks is also very low, except for r close to 191.99. Therefore, symbolic dynamics for the Lorenz map F can be well constructed for most of the parameters and F itself can be described by the extended geometric Lorenz map G to high accuracy.

5.3. *Predicting periodic windows of the Lorenz equations*

In order to demonstrate the power of the symbolic dynamics for the two-dimensional Lorenz map F and for the map G, we show how to predict new periodic windows in the Lorenz equations. However, it is tedious to work out the two-dimensional partitions for the map F, since one has to consider the backward sequences which always cause numerical difficulty of divergence. Fortunately, the Lorenz map F can be described by the extended geometric Lorenz map G rather well for most of the parameters and symbolic dynamics for map G is much simpler in the sense that only forward sequences are needed. Moreover, on the attractor, the map G is topologically equal to the map $f(u)$, so often one can deal with this one-dimensional case only. The ordering rules and admissibility conditions for the map $f(u)$ has already been given in (6) and (18).

The two symbolic sequences K_g and K_D determine the symbolic dynamics of the map $f(u)$ completely. When $K_D = \bar{K}_D = M^\infty$, $f(u)$ reduces to map (3). In what follows, we examine all symbolic sequences with length less than 7 to see which orbit should exist in the map $f(u)$.

Since the symbolic sequence in the map $f(u)$ is a subset of that of the one-dimensional antisymmetric cubic map (3), only symbolic sequences listed in Table 1 have to be considered. The condition $K_D > C$ makes all words containing a substring MM forbidden. This rules out 27 words and only leaves 23 that may be admissible in map $f(u)$. From these 23 words, only the following seven have not appeared in Table 2.

We check these seven words one by one. From Table 2 and the A value of the seven words, the word $RRLMR\bar{C}$ is located between the words $RRLMRMLLRML\bar{C}$ and $RRLML\bar{C}$, corresponding to $r = 143.4$ and 136.8, respectively. In the same way, we get possible r-ranges for other words in Table 5. Between $r = 143.4$ and 136.8, $K_D \approx RK_s$, so the word $RRLMR\bar{C}$ should exist in the Lorenz equations. Though we have not found the

stable periodic orbit $RRLMR\bar{C}$, we did obtain the unstable one at $r = 141.247$–141.249 by careful searching. Similarly, there is no rule to forbid the word $RRRLR\bar{C}$ and we have located it at $r = 76.818$–76.822. For the other five words, we have to determine K_D for each r-value carefully. Numerically, we find K_D by iterating the point with the greatest y-value in more than 10,000 points in the attractor in Σ. The result is listed in Table 6 in which we only present the first six letters for each K_D. In the range $r = 94.554$–99.275, K_D always begins with RR which make the substrings $MR\bar{C}$, $ML\bar{C}$, and $MLR\bar{C}$ forbidden. Thus the words $RRMR\bar{C}$, $RRML\bar{C}$, and $RRMLR\bar{C}$ would never appear in the Lorenz equations. Analogously, from K_D in Table 6 we can draw the conclusion that the other two words $RRRMR\bar{C}$ and $RRRMR\bar{C}$ are not admissible in the Lorenz equations.

In Table 6, as r decreases from $r = 130$, the difference between K_D and RK_s increases rapidly. On the other hand, up to $r = 60$, $K_D \approx K_g$. At $r = 40$ $K_D = R^{10}LRLRR \ldots$, which indicates that there is no stable period orbit with a period less than 10 for $r \leqslant 40$. We conjecture that when $r < 40$, $K_D < K_g$, no superstable periodic orbits may exist, though some periodic orbits with length greater than 10 can be stable. While r is small enough (say, $r < 30.1$), all the contracting part of the attractor is 'eaten' by K_D with $K_D \gg K_g$. No stable periodic orbits can be found and the Lorenz map F in the attractor is 'sufficiently' expanding. This is just the 'geometric Lorenz attractor' suggested by Guckenheimer and Williams [22, 21].

It should be noted that for r close to 191.99, the extended geometric Lorenz map G can not describe the Lorenz map F properly. The symbolic dynamics for the map F can not be well constructed. Many points fall into the region to the right of the dashed line in Fig. 14, which is the 'pruning' front determined by tangent points on the main branch of the

Table 5. Seven words that may be admissible but not listed in Table 2

No.	Period	Word	Possible r range	Existence
1	6	*RRLMR*	136.818–143.322	141.247–141.249
2	5	*RRMR*	94.554–99.275	forbidden by K_D
3	5	*RRML*	94.554–99.275	forbidden by K_D
4	6	*RRMLR*	94.554–99.275	forbidden by K_D
5	6	*RRRLR*	76.713–82.040	76.818–76.822
6	6	*RRRMR*	64.898–69.724	forbidden by K_D
7	6	*RRRML*	64.898–69.724	forbidden by K_D

Table 6. The K_D for different r-value for the Lorenz equations in $\sum$

No.	r	K_D	RK_s	K_g
1	209.5	*RLRCRM*	*RLMLRL*	*RMRLR*
2	199	*RLCLML*	*RLMLR*	*RMRLM*
3	192–130	$\geqslant RK_s$	RK_s	K_g
4	120	*RLMRR*	*RLRLR*	*RRLRLR*
5	110	*RLRMRR*	*RLLRLL*	*RRLRRL*
6	99	*RRLLCL*	*RLLMLL*	*RRMRRL*
7	98	*RRLLML*	*RLLMLL*	*RRMRRL*
8	97	*RRLLRM*	*RLLMLL*	*RRMRRL*
9	96	*RRLLRL*	*RLLMRR*	*RRMLLC*
10	95	*RRLLRL*	*RLLMRR*	*RRMLLC*
11	80	*RRMRRR*	*RLLLRL*	*RRRLRL*
12	70	*RRRLRL*	*RLLLRR*	*RRRRLL*
13	60	*RRRRLRR*	*RLLLLRL*	*RRRRLRR*
14	50	R^6LR	RL^6R	R^6LR
15	40	$R^{10}LR$	$RL^{10}R$	$R^{10}LR$

attractor. These points do not obey the admissibility conditions for the map G. We do find a 'non-cubic' word $RMLRMLMRL\bar{C}$ for the stable periodic orbit in the r range 191.985–191.982.

5.4. *Relation between the extended geometric Lorenz map G and the 'geometric Lorenz attractor'*

According to Guckenheimer and Holmes [22], the geometric Lorenz attractor is defined in Σ for $\sigma = 10$, $\beta = 8/3$, and $r \approx 28$. Based on an examination of the return map F, four additional assumptions are made. These assumptions can be expressed analytically. There is a system of coordinate, (u_g, v_g), on Σ. The curve u_g = constant is part of a strong stable foliation defined in a neighborhood of the attractor. This strong stable foliation is the MSM in our language. Then the return map G_g has the following properties.

1. The curves of MSM's are given by u_g = constant.
2. There are functions f_g and g_g such that G_g has the form $G_g(u, v) = (f_g(u_g), g_g(u_g, v_g))$ for $u_g \neq 0$ and $G_g(-u_g, -v_g) = -G_g(u_g, v_g)$.
3. $f'_g(u_g) > \sqrt{2}$ for $u_g \neq 0$ and $f'_g(u_g) \to \infty$ as $u_g \to 0$.
4. $0 < \partial g_g/\partial v_g < C < 1$ for $u_g \neq 0$ and $\partial g_g \to 0$ as $u_g \to 0$.

In Fig. 15, a scheme of the one-dimensional map f_g is shown. Denoting by R and L the regions to the right and to the left of the separating line D, the ordering rules can be written down as

$$PL \cdots < PR \ldots, \tag{21}$$

where P is an arbitrary string made of R and L, and the admissibility conditions for a word P which corresponds to a real trajectory in map G_g read [33]

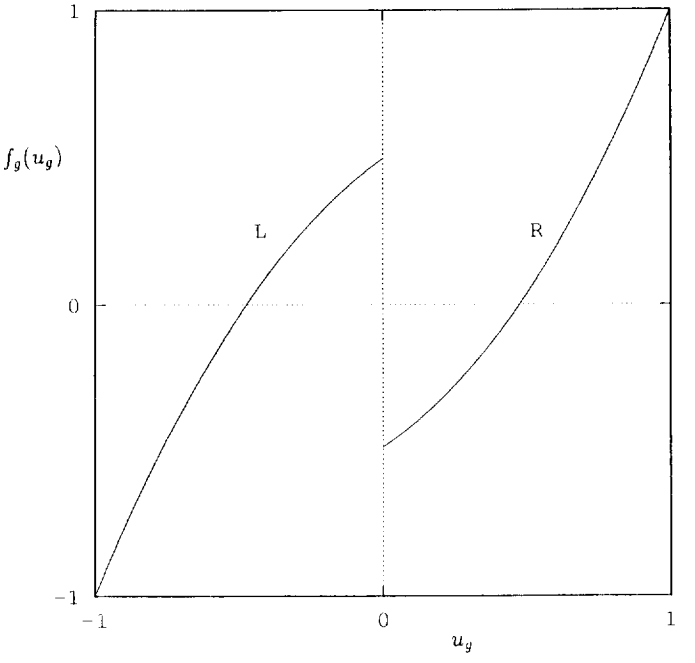

Fig. 15. The 1D map $f_g(u_g)$, inferred from the Lorenz map.

$$\begin{aligned} \mathscr{L}(P) &< K_D, \\ \bar{K}_D &< \mathscr{R}(P). \end{aligned} \tag{22}$$

The extended geometric Lorenz map G is defined in Σ for r big enough, say, $r > 46$, for which stable periodic orbits may appear at some parameters. The main difference between the assumptions for the extended geometric Lorenz map G and the geometric Lorenz map G_g is property (3). The return map G_g is 'sufficiently' expanding ($f_g'(u_g) > \sqrt{2}$) in the direction transverse to the MSM's, so that there are no tangent points in the attractor.

Our extended geometric Lorenz map G possesses tangencies between the MSM's and the BMSM's in the attractor. At the primary tangency $\bar{C}$ and C, $f'(u) = 0$ which allows the existence of stable periodic orbits. If we take the limit that $K_D > K_g$, the M part disappears. In this limit, the ordering rules and the the admissibility conditions for the symbolic sequences in map G are the same as that of the geometric Lorenz map. Furthermore, if K_D is sufficiently large that only the 'sufficiently' expanding part ($f'(u) > \sqrt{2}$) is left, $f(u)$ reduces to $f_g(u_g)$. Consequently, the geometric Lorenz attractor of Williams *et al.* is the limit of our extended geometric Lorenz attractor for K_D sufficiently large with $K_D > K_g$. At about $r = 30$, $K_D \gg K_g$. Below $r = 30$, the extended geometric Lorenz attractor becomes the geometric Lorenz attractor. This is the reason why we call the map G the 'extended' geometric Lorenz map.

6. DISCUSSION

Numerical investigation of many ordinary differential equations [34–39] as well as some partial differential equations [40–42], has revealed some similarity of the bifurcation structure with that of low-dimensional mappings. This has stimulated the application of symbolic dynamics of one-dimensional maps to the study of differential equations. The physical reason for low-dimensional symbolic dynamics working so well is of course the presence of dissipation, which causes the shrinking of phase space volume. Our work shows also the importance of symmetry in constructing symbolic dynamics for a physical system.

Recently, S. Smale summarized 10 great and unsolved problems in dynamical system theory [43], the first problem being the dynamics of the Lorenz equations (1), with $\sigma = 10$, $r = 28$, and $b = 8/3$, described by the 'geometric Lorenz attractor' of Williams *et al.* Our results push the problem into a much wider, obviously nonhyperbolic, range of parameter r. It seems that there is good hope to apply, rigorously or approximately, the method of symbolic dynamics to some nonhyperbolic systems and to add this method to the arsenal of practitioners in nonlinear dynamics.

Guckenheimer and Holmes indicated in their book [22] that nonhyperbolic limit sets are often encountered in examples of practical importance: "One would like to study their symbolic dynamics, but this has not been done in a satisfactory or systematic manner, except in the special case of mappings defined on the line." Our results on the Lorenz equations, though not being claimed to be satisfactory, do present a more or less systematic attempt in that direction.

Acknowledgements—The authors sincerely thank Drs Zheng Wei-mou, Gu Yan, Song Yan, Zhao Hong, Wu Zuo-bing, Liu Jiu-xie and Liu Zhong-hua for suggestions and discussion. BLH thanks the International Centre for Theoretical Physics, Trieste, where the final manuscript of this paper was written. This work was partially supported by the Chinese Natural Science Foundation and the Open Laboratories Project of Academia Sinica.

REFERENCES

1. B. Saltzman, Finite amplitude convection as an initial value problem, *J. Atoms. Sci.* **19**, 329 (1962).
2. L. N. Lorenz, Deterministic nonperiodic flow, *J. Atoms. Sci.* **20**, 130 (1963).
3. C. Sparrow, *The Lorenz Equations, Bifurcation, Chaos and Strange Attractors*. Springer, New York (1982).
4. M.-Z. Ding and B.-L. Hao, Systematics of the periodic windows in the Lorenz model and its relation with the antisymmetric cubic map, *Commun. Theor. Phys.* **9**, 375 (1988); reprinted in *Chaos II*, edited by B.-L. Hao, World Scientific, Singapore (1990).
5. M.-Z. Ding, B.-L. Hao and X. Hao, Power spectrum analysis and the nomenclature of periods in the Lorenz model, *Chinese Phys. Lett.* **2**, 1 (1985).
6. W.-M. Zheng and B.-L. Hao, Applied symbolic dynamics, in *Experimental Study and Characterization of Chaos*, Vol. 3 of *Directions in Chaos*, edited by B.-L. Hao, pp. 363–459. World Scientific, Singapore (1990).
7. F.-G. Xie and B.-L. Hao, Counting the number of periods in one-dimensioinal maps with mutliple critical points, *Physica A* **202**, 237 (1994).
8. M. Hénon, A two-dimensional mapping with strange attractors, *Commun. Math. Phys.* **50**, 69 (1976).
9. P. Grassberger and H. Kantz, Generating partitions for the dissipative Hénon map, *Phys. Lett. A* **113**, 235 (1985).
10. P. Cvitanović, G. H. Gunaratne and I. Procaccia, Topological and metric properties of Hénon-type strange attractors, *Phys. Rev. A* **38**, 1503 (1988).
11. P. Grassberger, H. Kantz and U. Moenig, On the symbolic dynamics of the Hénon map, *J. Phys. A* **22**, 5217 (1989).
12. H. Zhao, W.-M. Zheng and Y. Gu, Determination of partition lines from dynamical foliations for the Hénon map, *Commun. Theor. Phys.* **17**, 263 (1992).
13. H. Zhao and W.-M. Zheng, Symbolic analysis of the Hénon map at $a = 1.4$ and $b = 0.3$, *Commun. Theor. Phys.* **19**, 21 (1993).
14. L. Lozi, Un attracteur etrange du type attracteur de Hénon, *J Phys. (Paris) Colloq.* **39**, C5-9 (1978).
15. W.-M. Zheng, Symbolic dynamics for the Lozi map, *Chaos, Solitons & Fractals* **1**, 243 (1991).
16. W.-M. Zheng, Admissibility conditions for symbolic dynamics of the Lozi map, *Chaos, Solitons & Fractals* **2**, 461 (1992).
17. T. Tél, Invariant curves, attractors, and phase diagram of a piecewise linear map with chaos, *J. Stat. Phys.* **33**, 195 (1983).
18. W.-M. Zheng, Symbolic dynamics for the Tél map, *Commun. Theor. Phys.* **17**, 167 (1992).
19. K. Tomita and I. Tsuda, Towards the interpretation of the global bifurcation structure of the Lorenz system: a simple one-dimensional model, *Prog. Theor. Phys. Supp.* **69**, 185 (1980).
20. J. Guckenheimer and R. Williams, Structural stability of Lorenz attractors, *Publ. Math. IHES* **50**, 307 (1979).
21. R. Williams, The structure of Lorenz attractors, *Publ. Math. IHES* **50**, 101 (1979).
22. J. Guckenheimer and P. Holmes, Nonlinear oscillations, dynamical systems, and bifurcations of vector fields, in *Appl. Math. Science*, Vol. 42. Springer, New York (1983).
23. Y. Aizawa, Symbolic dynamics approach to intermittent chaos, *Progr. Theor. Phys.* **70**, 1249 (1983).
24. R. S. MacKay and C. Tresser, Some flesh on the skeleton: the bifurcation structure of bimodal maps, *Physica D* **27**, 412 (1987).
25. W.-M. Zheng and B.-L. Hao, Symbolic dynamics analysis of symmetry breaking and restoration, *Int. J. Mod. Phys. B* **3**, 1183 (1989).
26. N. Metropolis, M. L. Stein and P. R. Stein, On finite limit sets for transformations on the unit interval, *J. Combinat. Theor. A* **15**, 25 (1973).
27. H. Kantz and P. Grassberger, Repellers, semi-attractors, and long-lived chaotic transients, *Physica D* **17**, 75 (1985).
28. P. J. Holmes, A nonlinear oscillator with a strange attractor, *Phil. Trans. R. Soc. Lond. A* **292**, 419 (1979).
29. Y. Gu, Most stable manifolds and destruction of tori in dissipative dynamical system, *Phys. Lett. A* **124**, 340 (1987).
30. Y. Gu, Most stable manifolds and transition to chaos in dissipative dynamical system with competing frequencies, in *Directions in Chaos*, Vol. 2, edited by B.-L. Hao. World Scientific, Singapore (1988).
31. H.-P. Fang, Dynamics for strongly dissipative systems, *Phys. Rev. E* **49**, 5025 (1994).
32. H.-P. Fang, Symbolic dynamics for a two-dimensional antisymmetric map, *J. Phys. A* **27**, 5187 (1994).
33. W.-M. Zheng, Applied symbolic dynamics for the Lorenz-like map, *Phys. Rev. A* **42**, 2076 (1990).
34. O. E. Rossler, An equations for continuous chaos, *Phys. Lett. A* **57**, 397 (1976).
35. B.-L. Hao and S.-Y. Zhang, Hierarchy of chaotic bands, *J. Stat. Phys.* **28**, 769 (1982).
36. G.-R. Wang, B.-L. Hao and S.-Y. Zhang, U-sequences in the periodically forced Brusselator, *Commun. Theor. Phys.* **2**, 1075 (1983).
37. B.-L. Hao, Symbolic dynamics and systematics of periodic windows, *Physica A* **104**, 85 (1986).
38. B.-L. Hao, *Elementary Symbolic Dynamics and Chaos in Dissipative Systems*. World Scientific, Singapore (1989).
39. Y. Ueda, Survey of regular and chaotic phenomena in the forced Duffing oscillator, *Chaos, Solitons & Fractals* **1**, 199 (1991).
40. E. Knobloch, D. R. Moore, J. Toomre and N. O. Weiss, Transitions to chaos in two-dimensional double-diffusive convection, *J. Fluid Mech.* **166**, 409 (1986).

41. M. R. E. Proctor and N. O. Weiss, Normal forms and chaos in thermosolutal convection, *Nonlinearity* **3**, 619 (1990).
42. D. R. Moore and N. O. Weiss, Dynamics of double convection, *Phil. Trans. R. Soc. Lond. A* **332**, 121 (1990).
43. S. Smale, Dynamics retrospective: great problems, attempt that failed, *Physica D* **51**, 267 (1991).